Supporting Information

Water-Stable Lanthanide-Organic Macrocycles from 1,2,4-Triazole-based Chelate for Enantiomeric Excess Detection and Pesticide Sensing

Kai Cheng, [a,b] Qi-Xia Bai, [c] Shao-Jun Hu, [a,b] Xiao-Qing Guo, [a,b] Li-Peng Zhou, [a] Ting-Zheng Xie, [c] and Qing-Fu Sun*[a, b]

[a] State Key Laboratory of Structural Chemistry, Fujian Institute of Research on the Structure of Matter, Chinese Academy of Sciences, Fuzhou 350002, PR China.

[b] University of Chinese Academy of Sciences, Beijing 100049, PR China.

[c] Institute of Environmental Research at Greater Bay Area; Key Laboratory for Water Quality and Conservation of the Pearl River Delta, Ministry of Education; Guangzhou Key Laboratory for Clean Energy and Materials; Guangzhou University, Guangzhou 510006, China.

Contents

1 General

Unless otherwise stated, all chemicals and solvents were purchased from commercial companies and used without further purification. Anhydrous solvents were distilled according to standard procedures. Deuterated solvents were purchased from Adamas, J&K scientific and Sigma-Aldrich. 1D and 2D NMR spectra were measured on a Bruker Biospin Avance III (400 MHz) spectrometer and JEOL ECZ600S (600 MHz) spectrometer. ^{1}H-NMR chemical shifts were determined with respect to residual signals of the deuterated solvents used. Mass spectral data were collected by three different instruments. Electro-spray-ionization time-of-flight mass-spectroscopy (ESI-TOF-MS) were recorded on an Impact II UHR-TOF mass spectrometry from Bruker, with tuning mix as the internal standard. Data analysis was conducted with the Bruker Data Analysis software (Version 4.3) and simulations were performed with the Bruker Isotope Pattern software. ESI mass spectrometry (MS) experiments were performed on a Waters Synapt HDMS G2-Si quadrupole/time-of-flight (Q/TOF) tandem mass spectrometer. This instrument contains a triwave device between the Q and TOF analyzers, consisting of three collision cells in the order trap cell, ion mobility cell, and transfer cell. Trap and transfer cells are pressurized with Ar, and the ion mobility cell is pressurized with N_2 flowing in a direction opposite to that of the entering ions. Some MS spectra were recorded on LC-QTOF-MS from Agilent. Excitation and emission spectra were recorded on the FS5 spectrofluorometer from Edinburg Photonics. Spectra were corrected for the experimental functions. The emission quantum yields in solution were measured on FS5 with an SC-30 Integrating Sphere. For liquid samples the reference would be a cuvette containing the solvent only. UV-Vis spectra are recorded on UV-2700 spectrophotometer from SHIMADZU.

2 Synthesis and characterization

2.1 Synthetic procedures

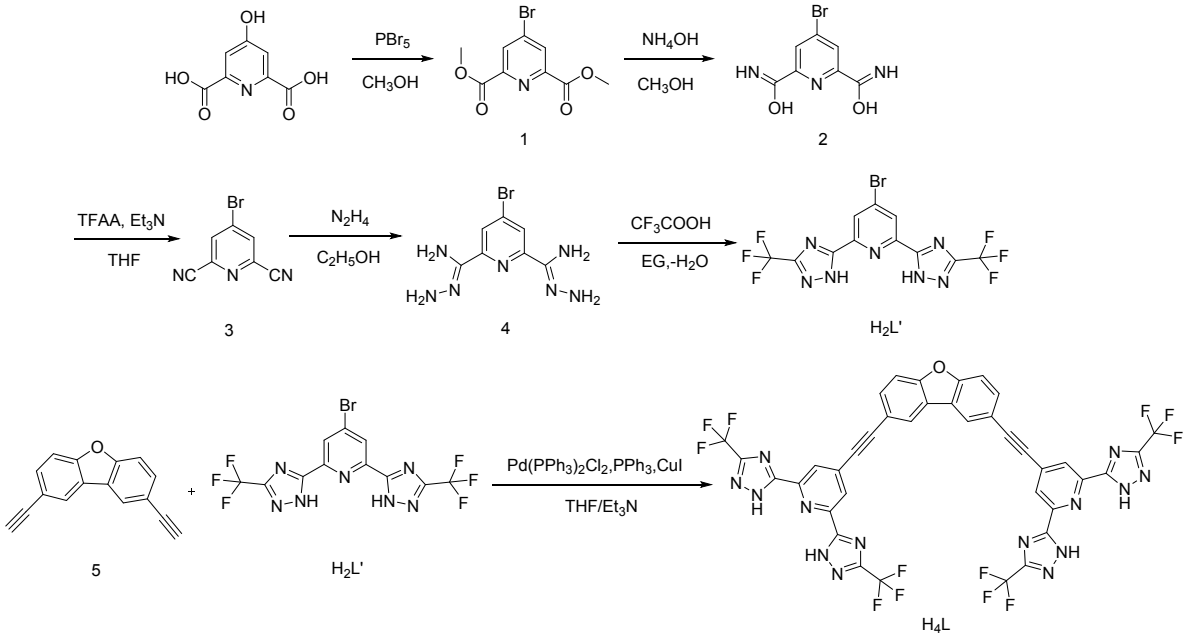

Scheme S1. The synthetic route of ligands $\mathbf{H_2L}$' and $\mathbf{H_4L}$.

The preparation of compound **1**, **5** followed the literature procedure.[1,2] Ligand $\mathbf{H_2L}$' was synthesized by optimizing the original method reported in the literature. [3]

Synthesis of 2

To a solution of dimethyl 4-bromopyridine-2, 6-dicarboxylate (6.2 g, 22.62 mmol, 1.0 eq.) in MeOH (80 ml), DCM (20 ml) and ammonia solution (33 wt.%, 20 ml) were added and the reaction was stirred at room temperature overnight. The precipitation was filtered, washed with minimum amount of DCM and MeOH, and then dried in vacuum to give **2** as white solid. (4.3 g, 78% yield). ^{1}H NMR (400 MHz, d_6-DMSO) δ 8.92 (s, 2H), 8.30 (s, 2H), 7.88 (s, 2H).^{13}C NMR (101 MHz, d_6-DMSO) δ 164.52, 150.92, 135.38, 127.46. HR-MS (ESI) calcd. for $C_7H_6BrN_3O_2$ $[M+Na]^+$:265.9536, found 265.9523.

Synthesis of 3

To a solution of **2** (1.92 g, 7.87 mmol, 1.0 eq.) and anhydrous triethylamine (2.5 ml, 17.33 mmol, 2.2 eq.) in anhydrous THF (25 ml), trifluoroacetic anhydride (2.5 ml, 17.33 mmol, 2.2 eq.) was added slowly at 0℃. The reaction was stirred at room temperature for 12 h and then it was quenched by adding saturated sodium bicarbonate solution. The precipitation was filtered, washed with water, and then dried in vacuum to give **3** as white solid. (1.47 g, 90% yield). ^{1}H NMR (400 MHz, $CDCl_3$) δ 8.07 (s, 2H).^{13}C NMR (101 MHz, $CDCl_3$) δ 135.24, 134.30, 114.42. HR-MS (ESI) calcd. for $C_7H_2BrN_3$ $[M+NH_4]^+$:224.9770, found 224.9468.

Synthesis of 4

A mixture of **3** (0.8 g, 5.4 mmol, 1.0 eq.) and hydrazine hydrate (5.2 ml, 108 mmol, 20 eq.) in ethanol (55.0 mL), was stirred at 75 ºC for 12 h. The precipitation was filtered, washed with anhydrous ethanol, and then dried in vacuum to give **4** as pale yellow solid. (1.40g, 95% yield). ^{1}H NMR (400 MHz, d_6-DMSO) δ 7.91 (s, 2H), 6.10 (s, 4H), 5.41 (s, 4H). ^{13}C NMR (101 MHz, d_6-DMSO) δ 152.49, 142.63, 131.75, 120.65. HR-MS (ESI) calcd. for $C_7H_{10}BrN_7$ $[M+Na]^+$:294.0073, found 294.0012.

Synthesis of H_2L'

To **4** (0.68 g, 2.5 mmol, 1.0 eq.) in trifluoroacetic acid (20.0 mL), the reaction was stirred at 75ºC for 12 h. The solvent was removed under reduced pressure, then ethylene glycol (10 mL) was added, the reaction was stirred at 130 ºC for 4 h, cooled to room temperature. Excess of H_2O (50 mL) was added and a precipitate was formed, filtered off and dried, the crude product was purified by flash chromatography (SiO_2, DCM: EA=5:1) to afford **H_2L'** as a white powder. (0.83 mg, 78% yield). ^{1}H NMR (400 MHz, CD_3CN) δ 8.41 (s, 2H).^{19}F NMR (376 MHz, CD_3CN) δ -65.92 (s, 6F).^{13}C NMR (101 MHz, CD_3CN) δ 154.82, 146.54, 136.27, 126.65, 121.34, 118.67. HR-MS (ESI) calcd. for $C_{11}H_4BrF_6N_7$ $[M-H]^-$: 425.9543, found 425.9508.

Synthesis of H_4L

A mixture of **H_2L'** (1.00 g, 2.33 mmol, 2.2 eq.), **5** (216 mg, 1 mmol, 1.0 eq.), $Pd(PPh_3)_2Cl_2$ (70 mg, 0.10 mmol, 0.1 eq.), CuI (38 mg, 0.20 mmol, 0.2 eq.) and PPh_3 (53 mg, 0.20 mmol, 0.2 eq.) in tetrahydrofuran (35 mL) and triethylamine (35 mL), was stirred at 66°C for 1 day under nitrogen atmosphere. After cooling to room temperature, the solvent was removed under reduced pressure, and the crude product was purified by flash chromatography on silica gel treated with triethylamine (DCM/CH_3OH, 10:1) to afford **H_4L** (500mg, 55% yield) as white solid. ^{1}H NMR (400 MHz, d_6-DMSO) δ 8.65 (s, 2H), 8.00 (s, 4H), 7.97 – 7.90 (dd, 4H).^{19}F NMR (376 MHz, d_6-DMSO) δ -61.36 (s, 12F).^{13}C NMR (101 MHz, d_6-DMSO) δ 162.04, 156.81, 154.32, 153.98, 150.63, 126.35, 124.00, 123.55, 120.87, 119.66, 117.02, 113.29, 86.87. HR-MS (ESI) calcd. for $C_{38}H_{14}F_{12}N_{14}O$ $[M-H]^-$:909.1211, found 909.1037.

Synthesis of La_2L_2

H_4L (10 mg, 10.1 μmol, 1.00 eq.) was treated with $La(OTf)_3$ (5.9 mg, 10.1 μmol, 1.00 eq.) in DMSO, then triethylamine (5.8 μL, 42.4 μmol, 4.2 eq.) was added at 50°C and stirred for 10 minutes, a homogeneous colorless solution was obtained. ^{1}H NMR (400MHz, d_6-DMSO, 298K) δ 8.66 (s, 4H), 8.09 (s, 8H), 7.95 (br, 8H). ^{19}F NMR (376 MHz, d_6-DMSO) δ -61.71 (s, 24F).^{13}C NMR was not measured due to the poor solubility of such complexes. HR-MS (ESI) calcd. for $[La_2L_2]^{2-}$ 1044.9373, found 1045.0034.

Synthesis of Eu_2L_2

H_4L (10 mg, 10.1 μmol, 1.00 eq.) was treated with $Eu(OTf)_3$ (6.0 mg, 10.1 μmol, 1.00 eq.) in DMSO, then triethylamine (5.8 μL, 42.4 μmol, 4.2 eq.) was added at 50°C and stirred for 10 minutes, a homogeneous colorless solution was obtained. ^{1}H NMR (400MHz, d_6-DMSO, 298K) δ 8.36 (s, 4H), 7.81 (br, 4H), 7.72 (br, 4H), 5.17 (s, 8H).

^{19}F NMR (376 MHz, d_6-DMSO) δ -63.21(s, 24F). ^{13}C NMR was not measured due to the poor solubility of such complexes. HR-MS (ESI) calcd. for $[Eu_2L_2]^{2-}$ 1115.0280, found 1115.0360.

2.2 NMR spectra

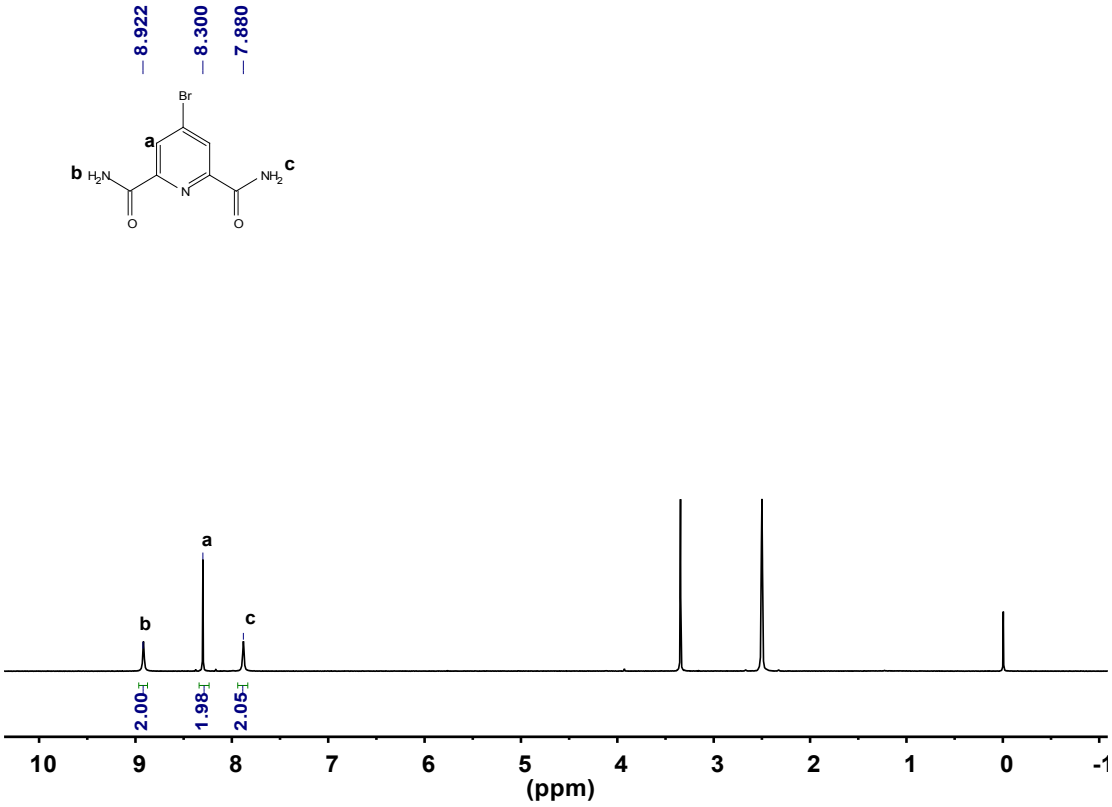

Figure S1. ^{1}H NMR spectrum of **2** (400 MHz, DMSO-d_6, 298 K).

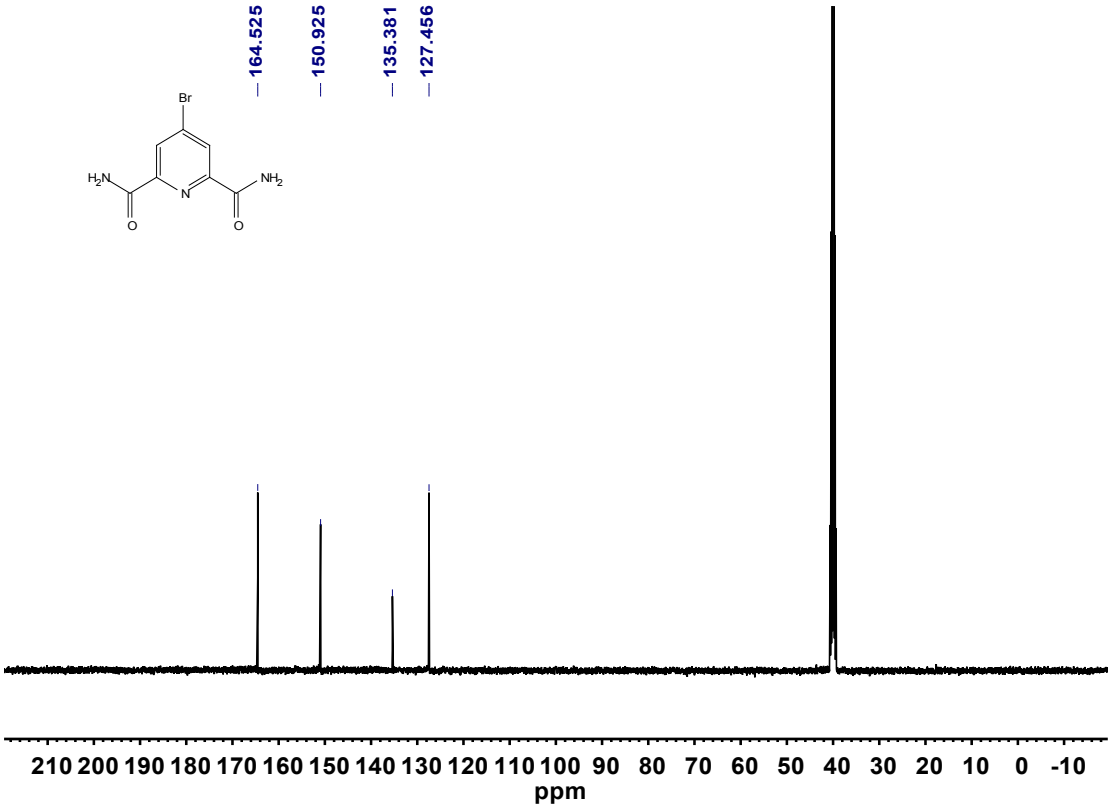

Figure S2. ^{13}C NMR spectrum of **2** (101MHz, DMSO-d_6, 298 K).

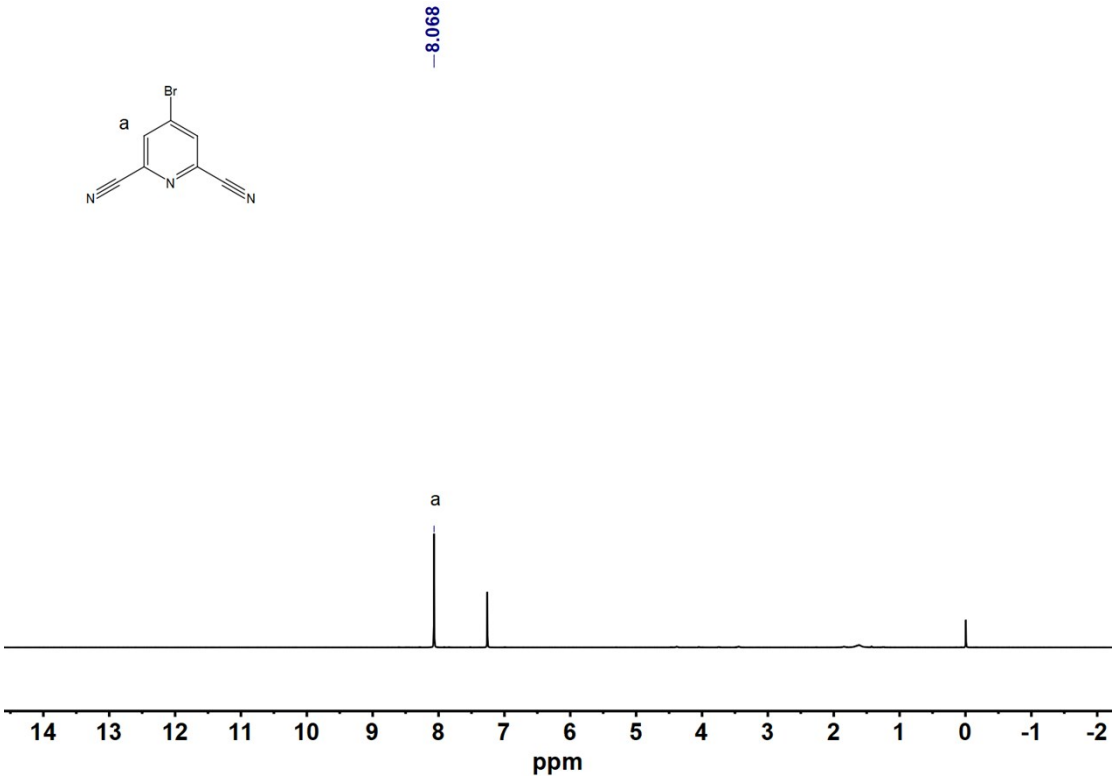

Figure S3. ^{1}H NMR spectrum of **3** (400 MHz, $CDCl_3$, 298 K).

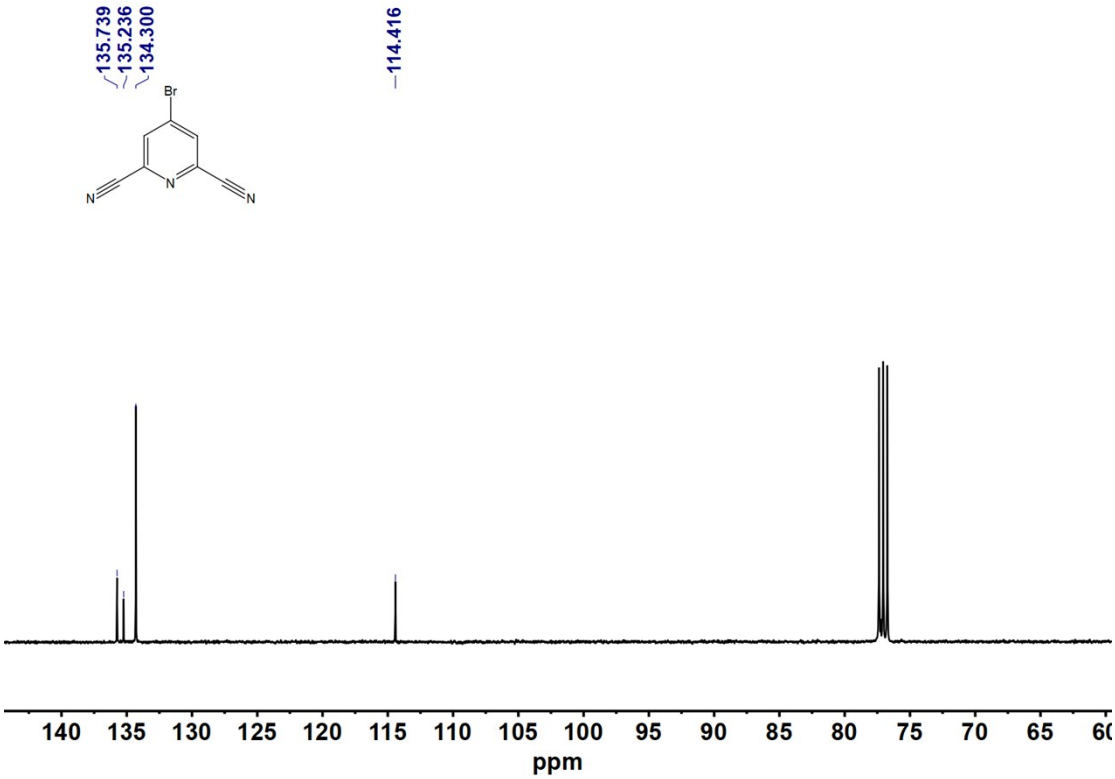

Figure S4. ^{13}C NMR spectrum of **3** (101 MHz, $CDCl_3$, 298 K).

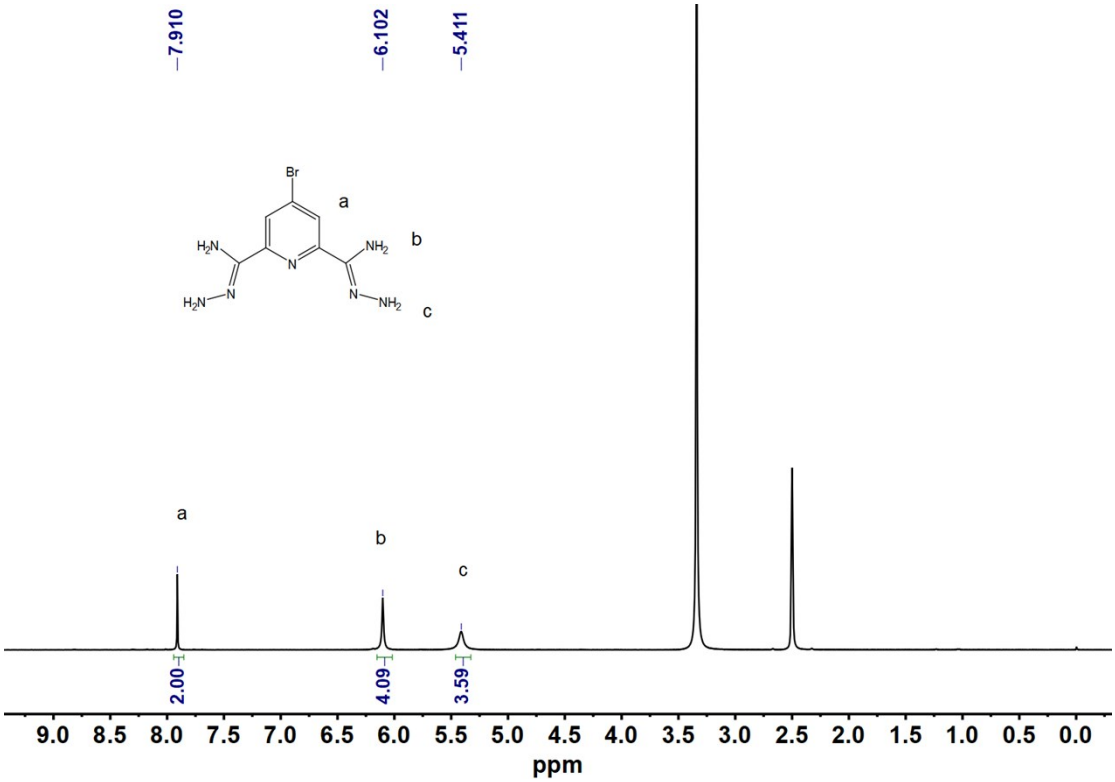

Figure S5. ^{1}H NMR spectrum of **4** (400 MHz, DMSO-d_6, 298 K).

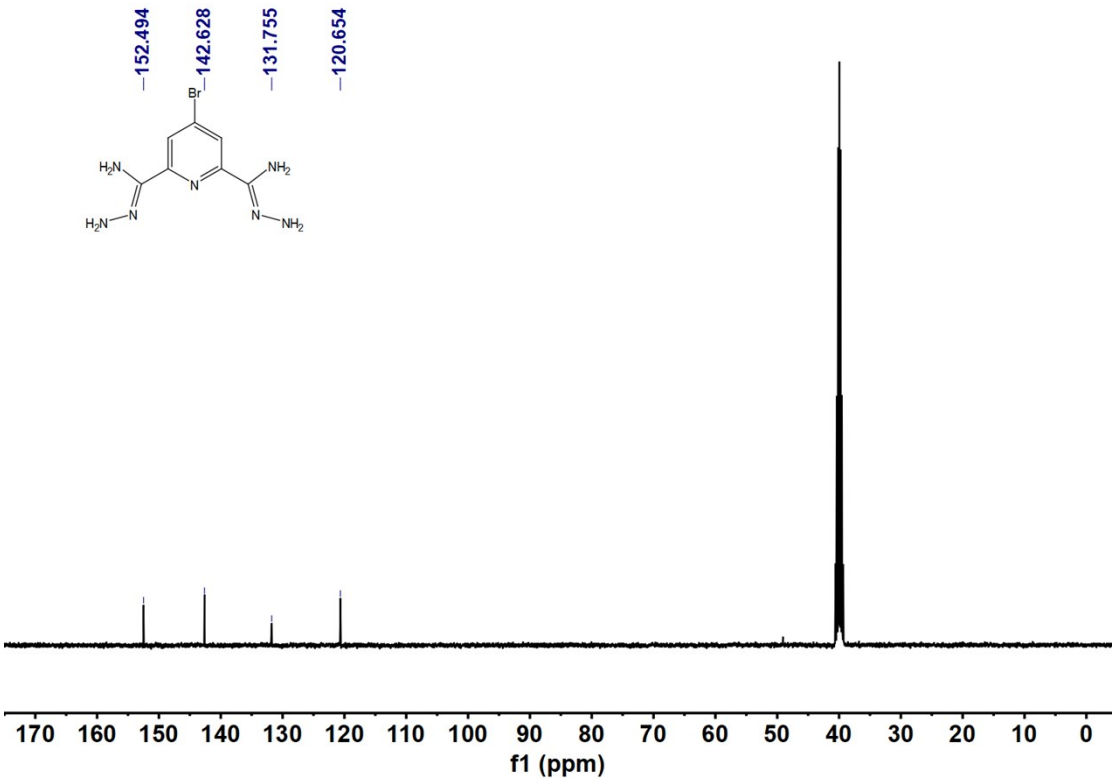

Figure S6. ^{13}C NMR spectrum of **4** (101 MHz, DMSO-d_6, 298 K).

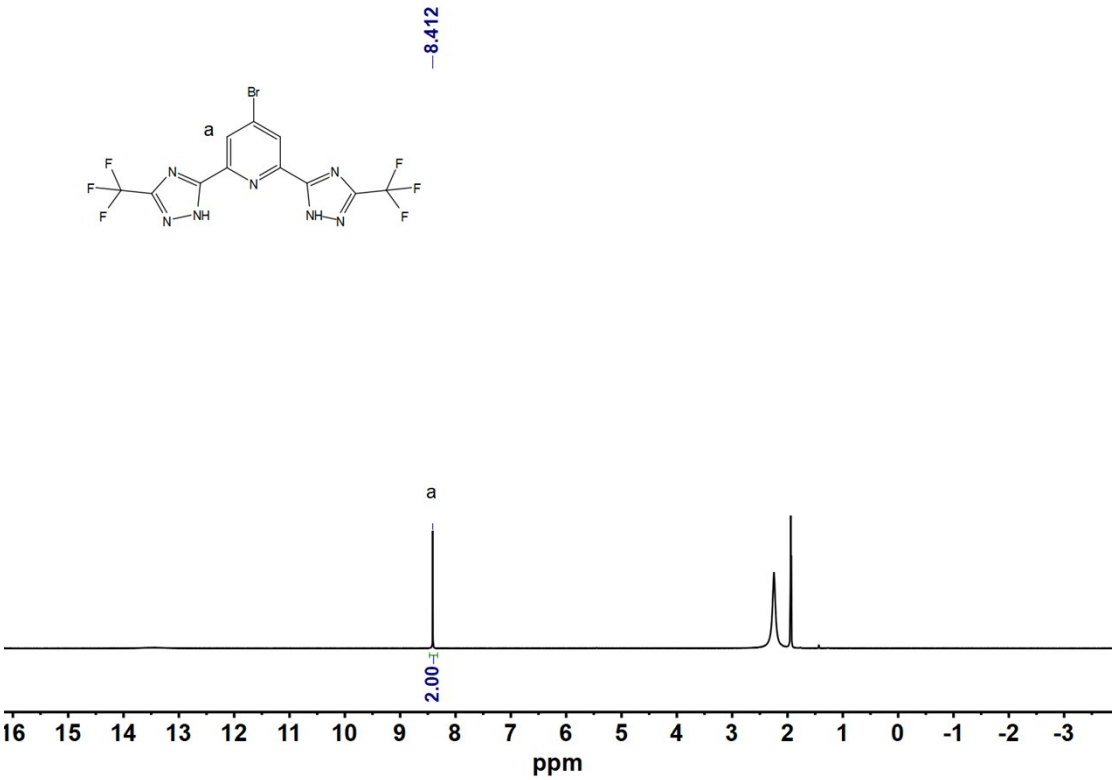

Figure S7. ^{1}H NMR spectrum of **5** (400 MHz, CD_3CN, 298 K).

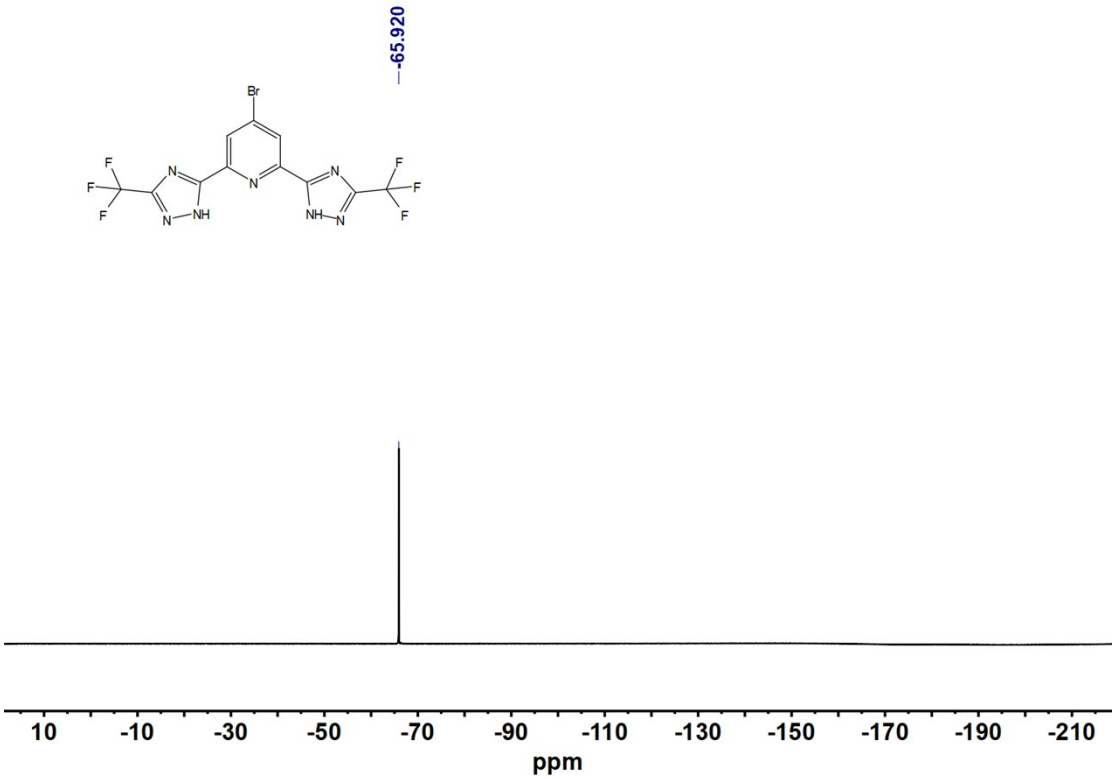

Figure S8. ^{19}F NMR spectrum of **H_2L'** (376 MHz, CD_3CN, 298 K).

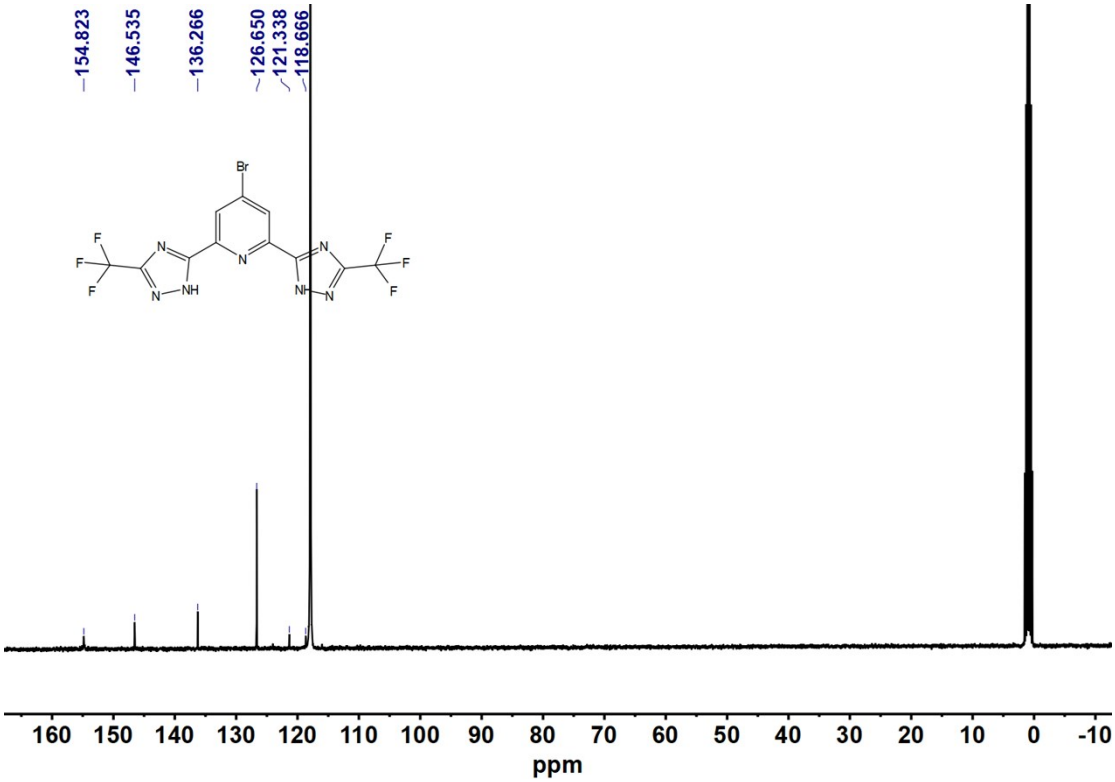

Figure S9. ^{13}C NMR spectrum of **H_2L'** (101 MHz, CD_3CN, 298 K).

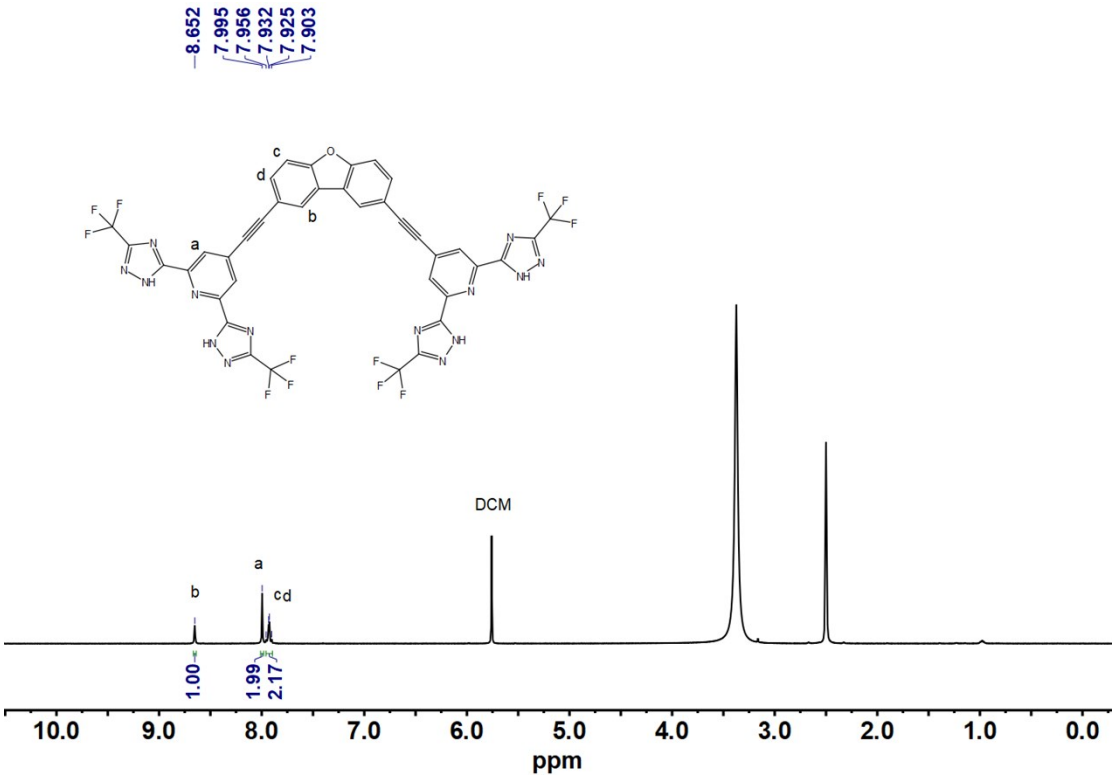

Figure S10. ^{1}H NMR spectrum of **H_4L** (400 MHz, DMSO-d_6, 298 K).

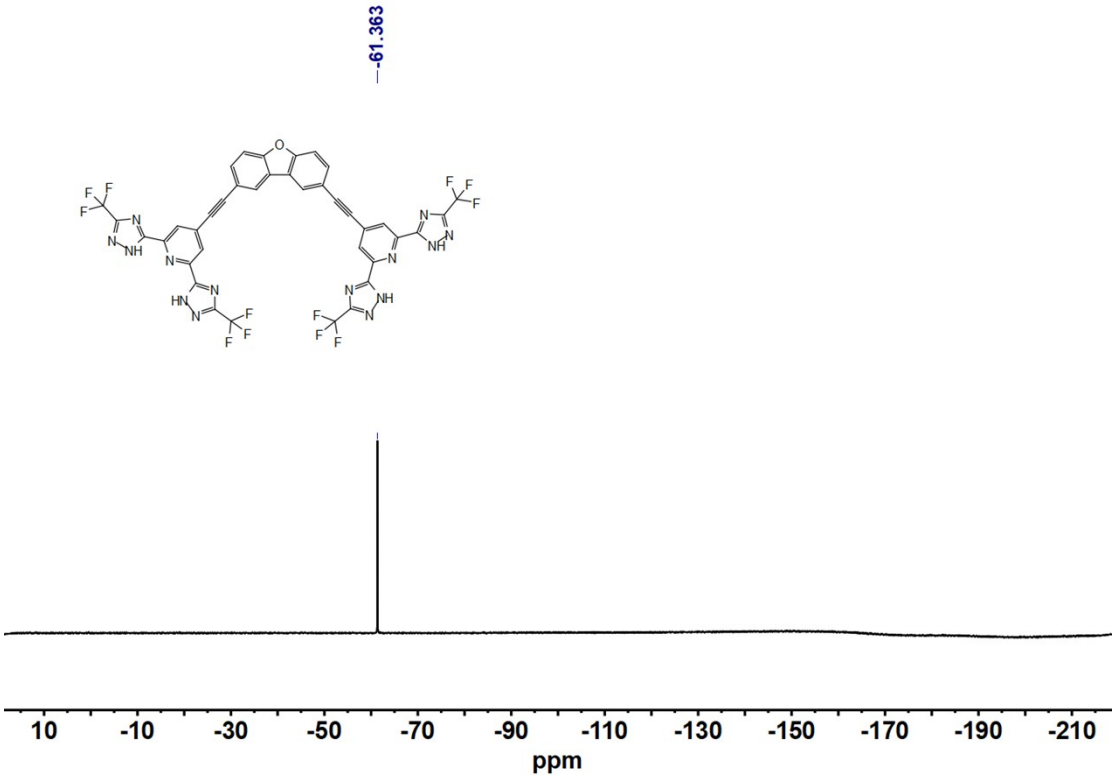

Figure S11. ^{19}F NMR spectrum of **H_4L** (376 MHz, DMSO-d_6, 298 K).

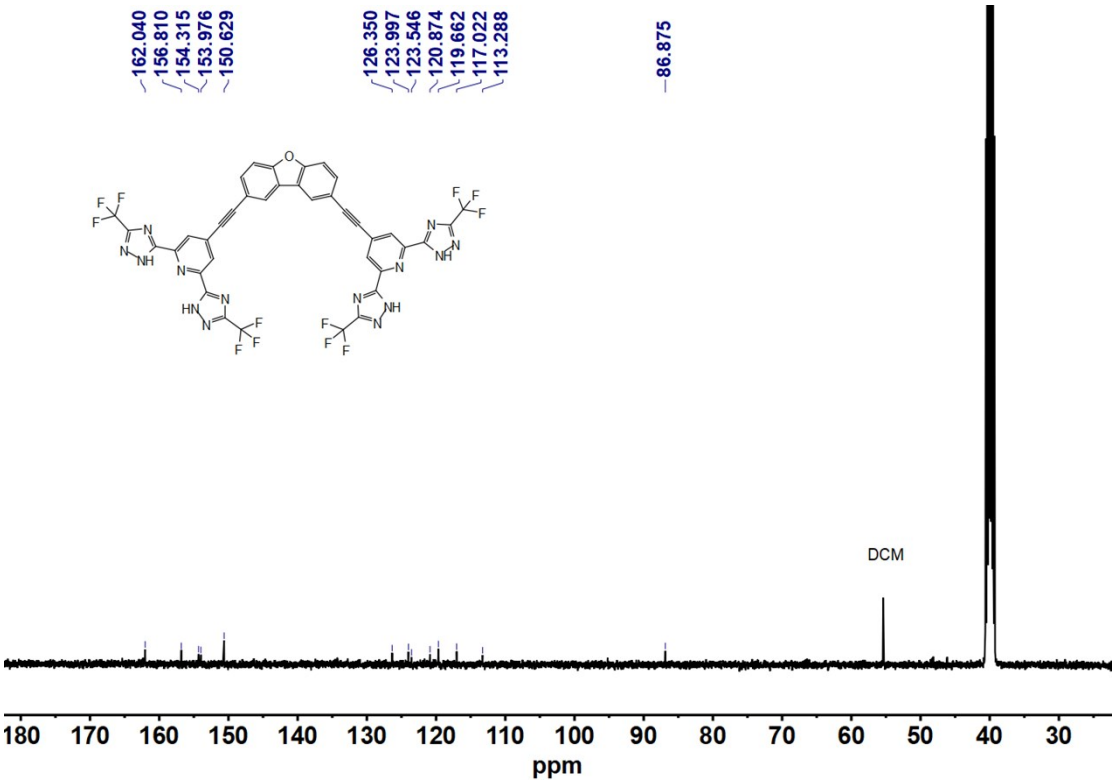

Figure S12. ^{13}C NMR spectrum of **H_4L** (101 MHz, DMSO-d_6, 298 K).

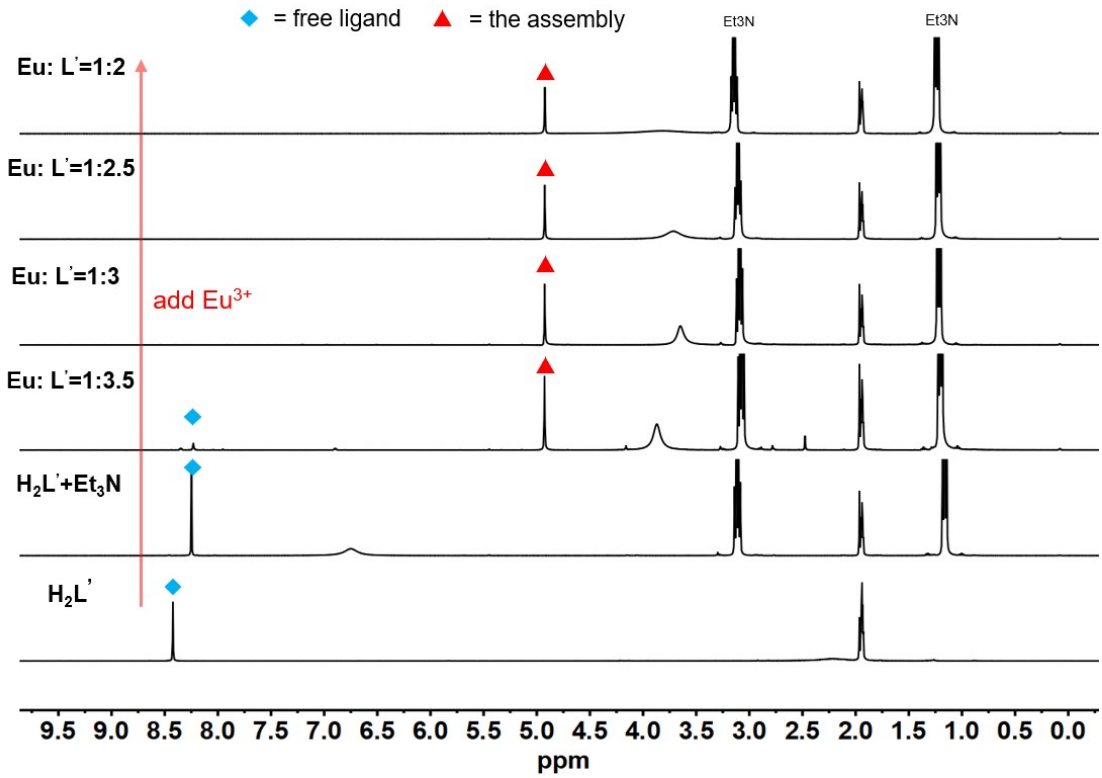

Figure S13. ^1H NMR (400 MHz, 298 K) titration spectra of titrating **H_2L'** and triethylamine with $Eu(OTf)_3$ in CD_3CN.

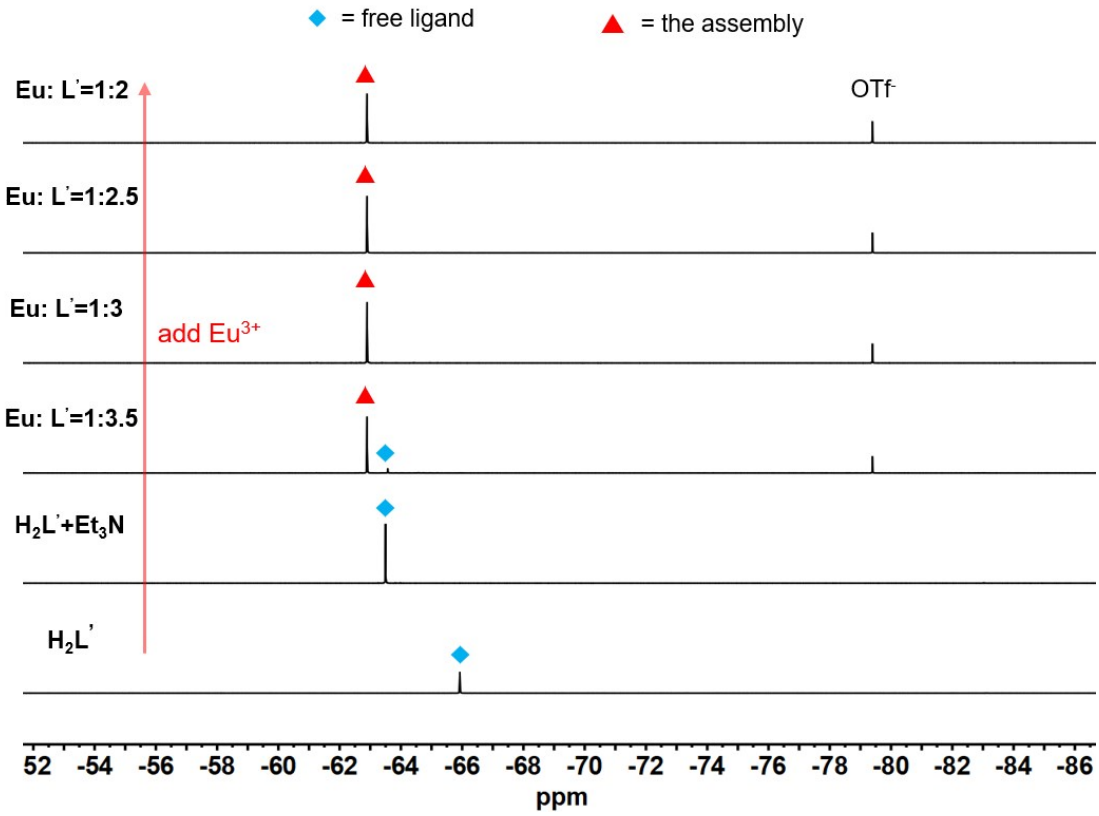

Figure S14. ^{19}F NMR (376 MHz, 298 K) titration spectra of titrating **H_2L'** and triethylamine with Eu(OTf)$_3$ in CD_3CN.

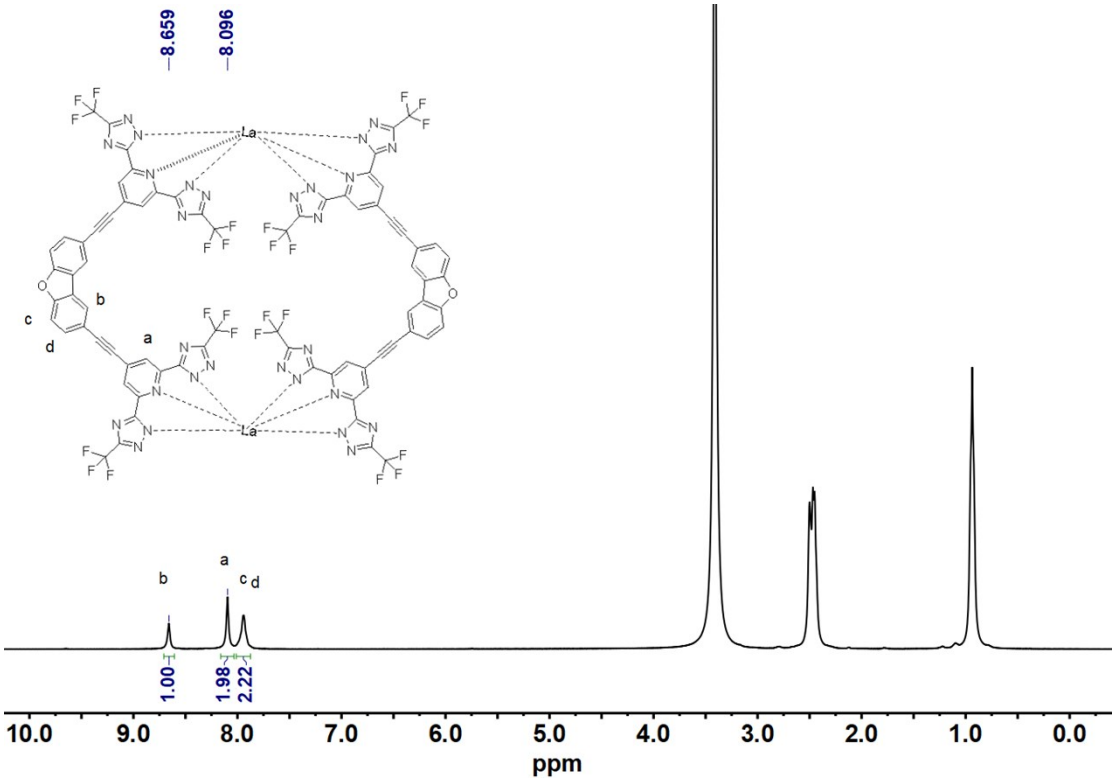

Figure S15. ^{1}H NMR spectrum of **La_2L_2** (400 MHz, DMSO-d_6, 298 K).

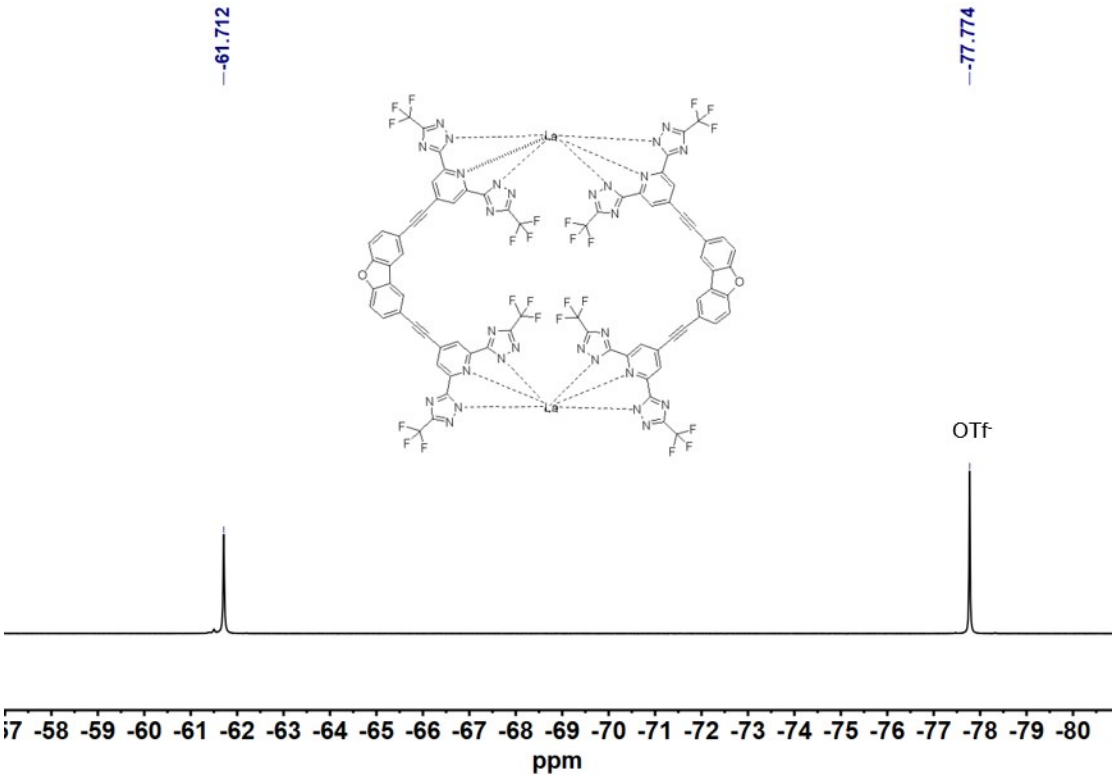

Figure S16. ^{19}F NMR spectrum of **La_2L_2** (376 MHz, DMSO-d_6, 298 K).

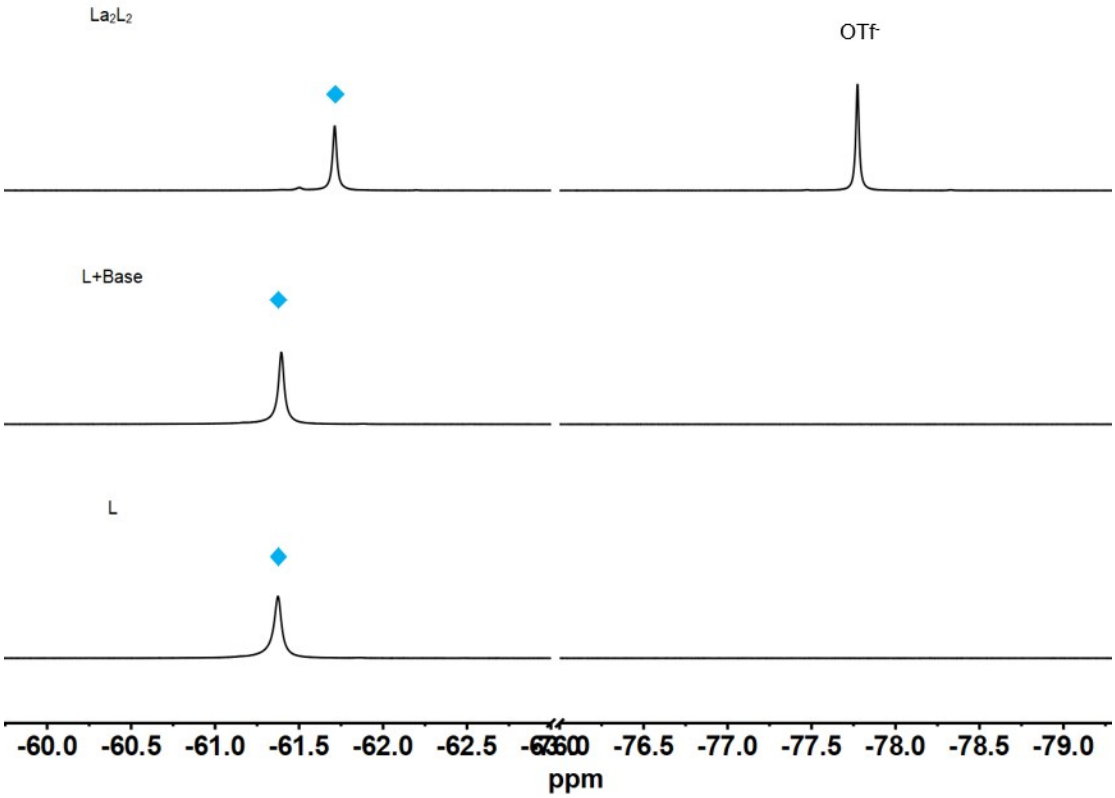

Figure S17. Comparison of ^{19}F NMR spectra of **H_4L**, **H_4L** with Et_3N and **La_2L_2** (376 MHz, DMSO-d_6, 298 K).

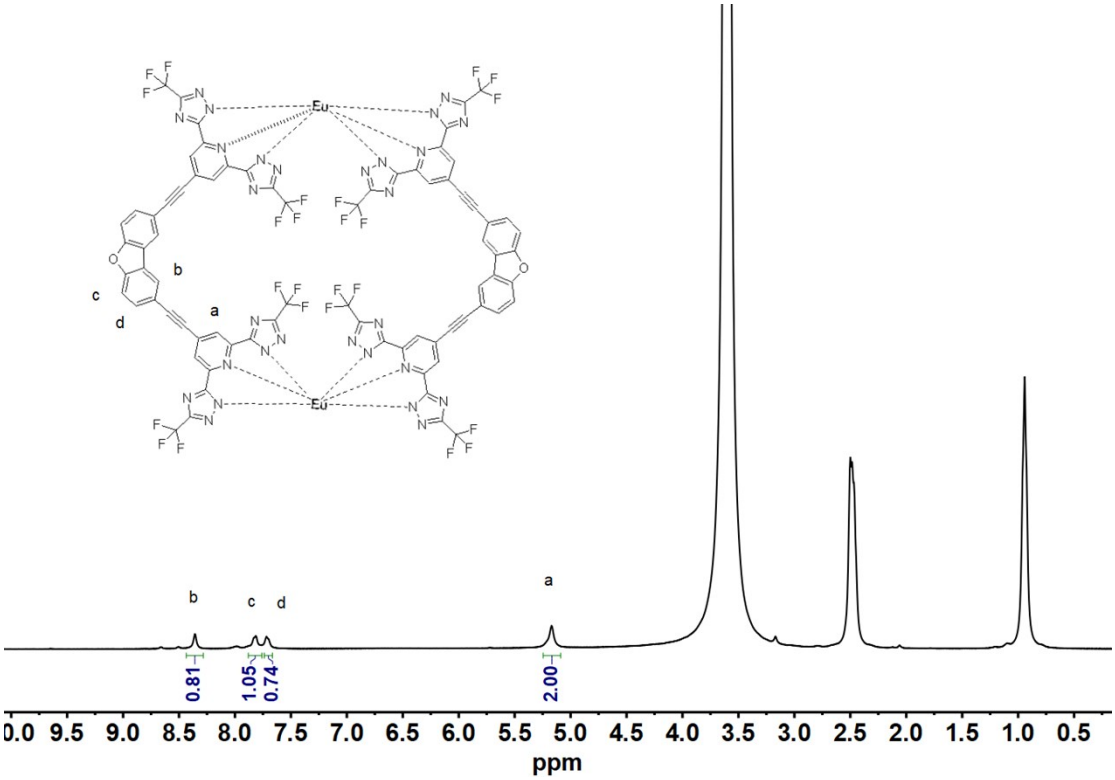

Figure S18. ^{1}H NMR spectrum of $\mathbf{Eu_2L_2}$ (400 MHz, DMSO-d_6, 298 K).

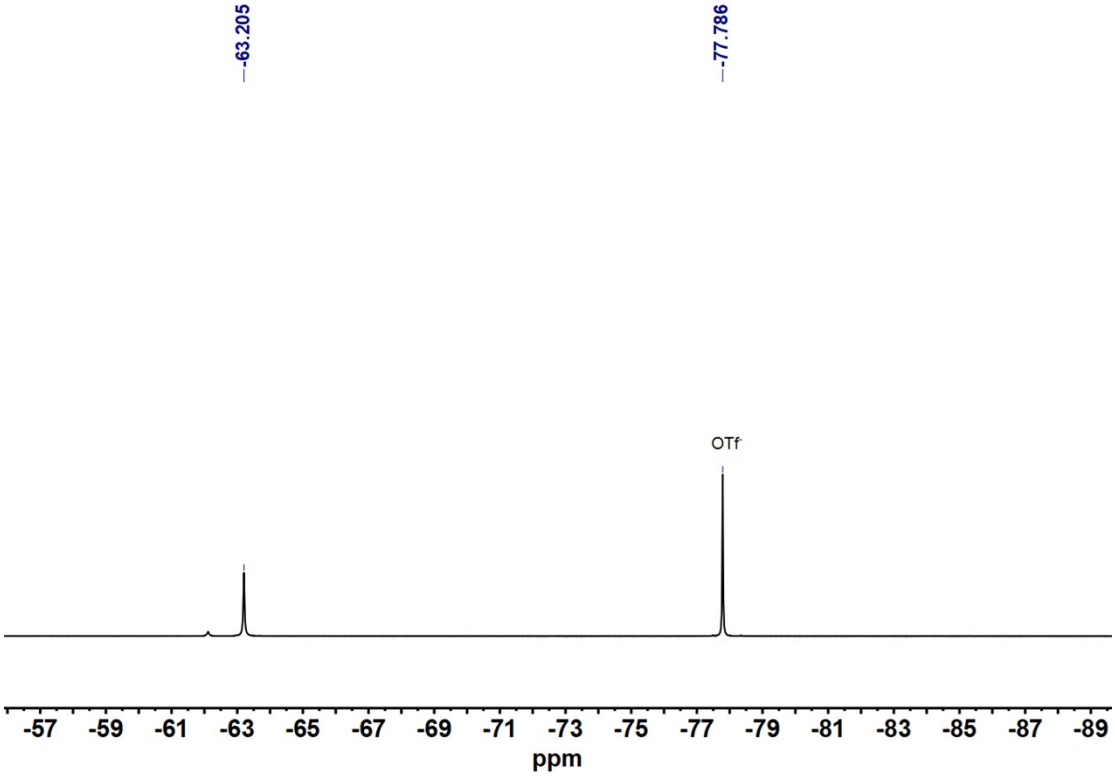

Figure S19. ^{19}F NMR spectrum of $\mathbf{Eu_2L_2}$ (376 MHz, DMSO-d_6, 298 K).

2.3 ^{1}H DOSY spectra

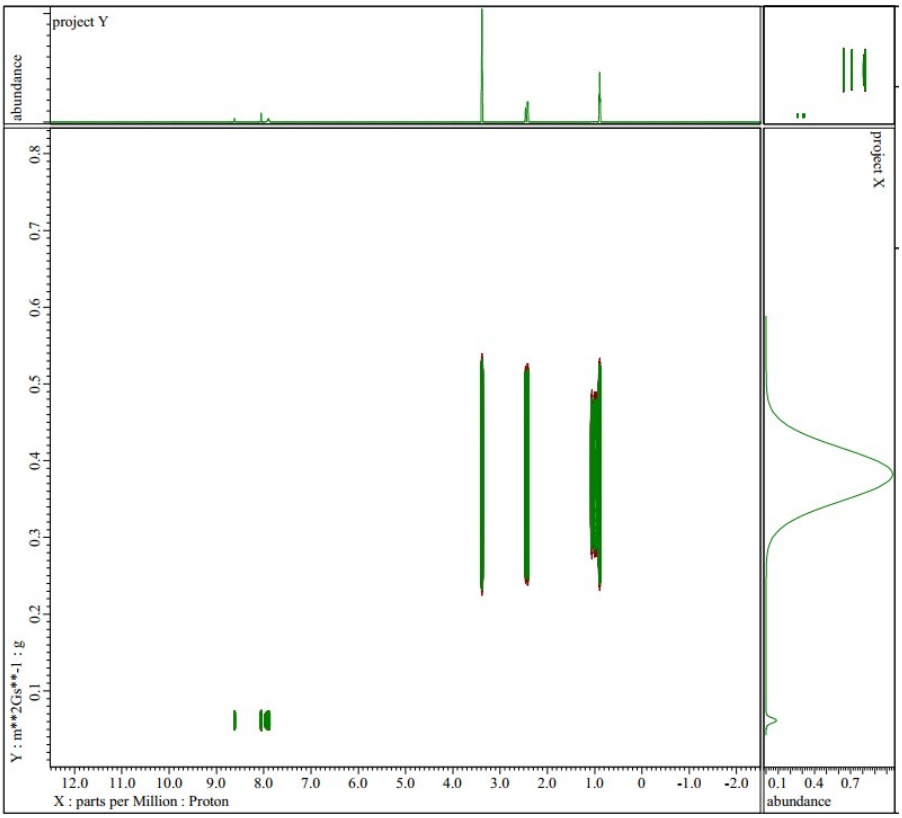

Figure S20. ^{1}H DOSY spectrum of **La_2L_2** (600 MHz, DMSO-d_6, 298 K, D=6.08×10^{-11} m^2·s^{-1})

3 Photophysical properties

3.1 UV-Vis absorption and Luminescence Spectra

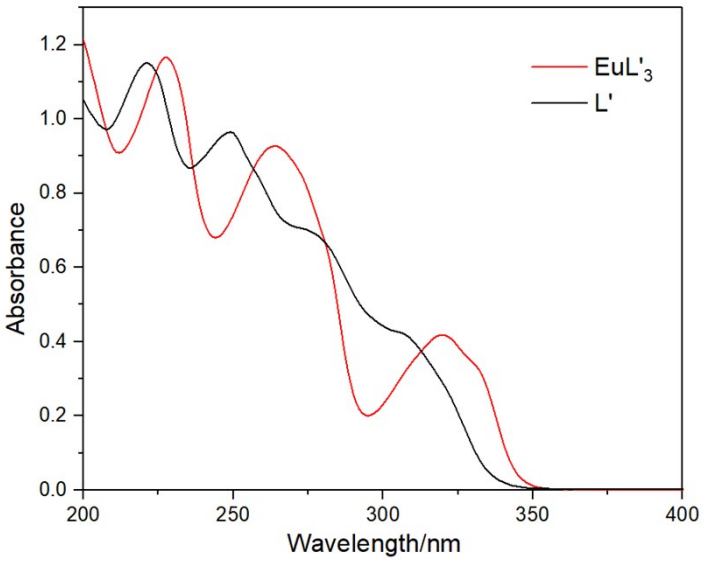

Figure S21. UV/Vis absorption spectra of L' with equivalent Et_3N(c = 6.0×10^{-5} M), EuL'$_3$(c = 2.0×10^{-5} M) in CH_3CN.

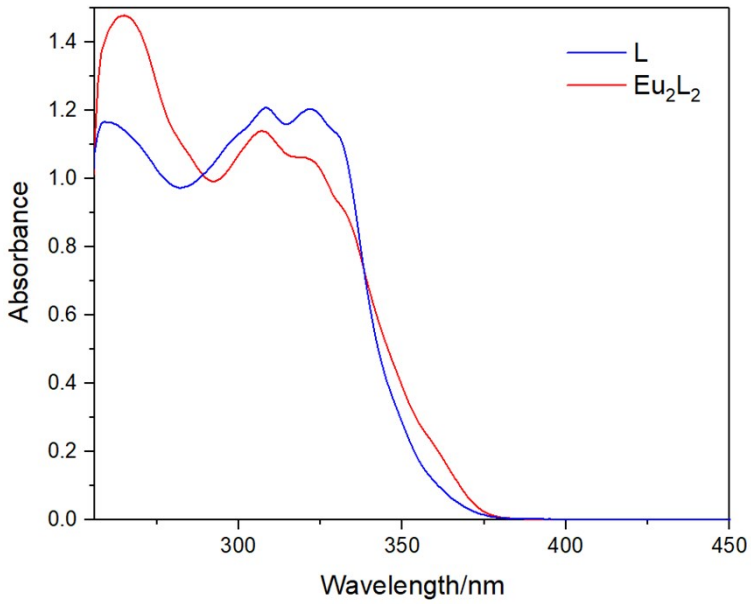

Figure S22. UV/Vis absorption spectra of H_4L with equivalent Et_3N(c = 2.0×10^{-5} M) and Eu_2L_2 (c = 1.0×10^{-5} M) in DMSO.

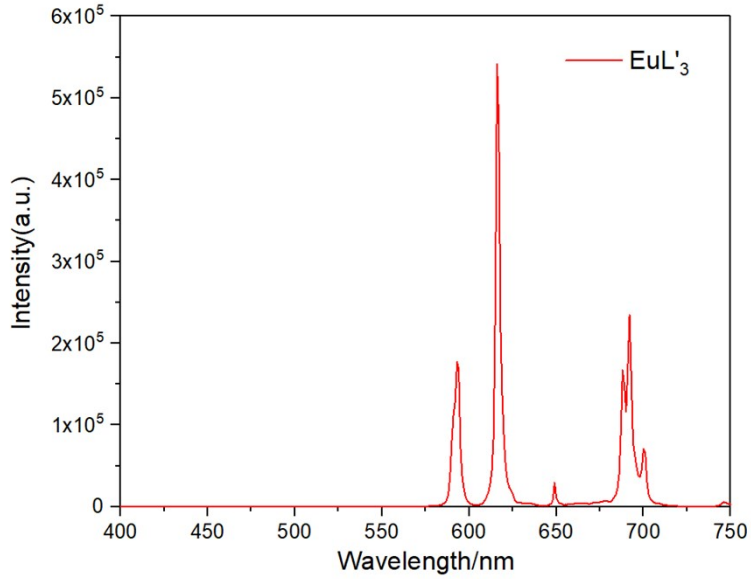

Figure S23. Emission spectrum of EuL'$_3$ (c = 2×10^{-5} M, λ_{ex} = 264 nm, slits = 1.2 – 0.8).

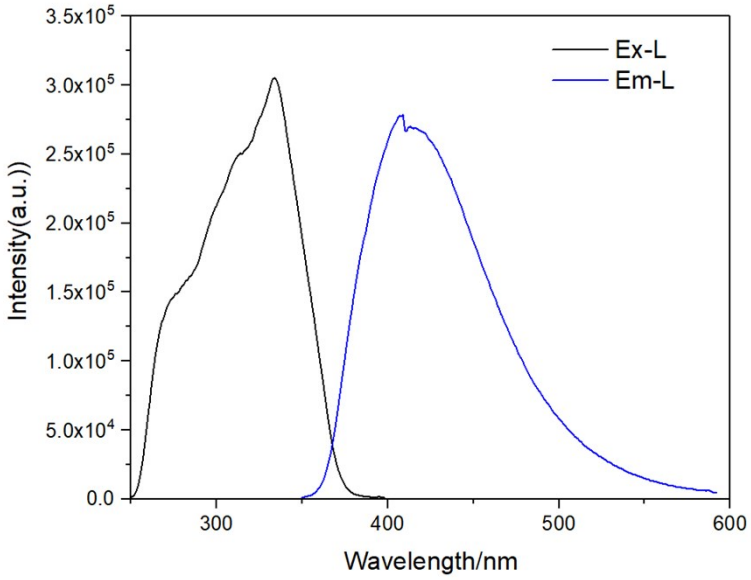

Figure S24. Excitation spectrum (black lines) and emission spectrum (blue lines) of L with equivalent Et_3N in DMSO ($c = 2\times10^{-5}$ M, $\lambda_{em} = 406$nm, $\lambda_{ex} = 334$ nm, slits = 4-1.8).

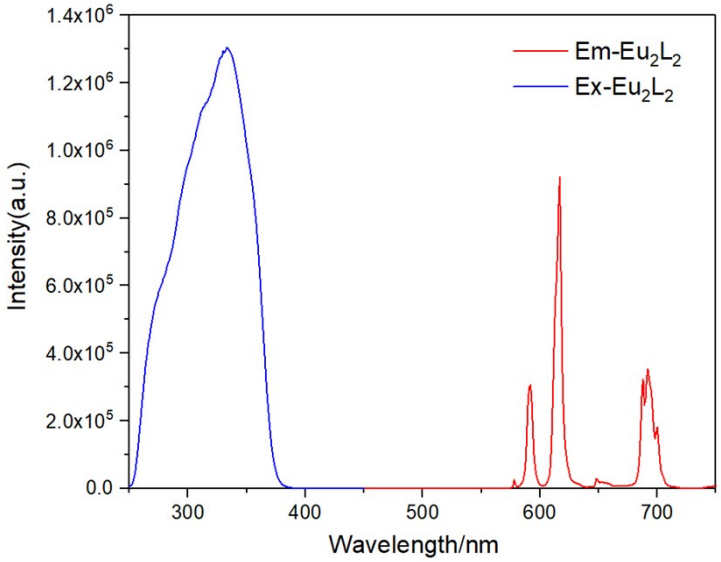

Figure S25. Excitation spectrum (blue lines) and emission spectrum (red lines) of Eu_2L_2 in DMSO ($c = 1\times10^{-5}$ M, $\lambda_{em} = 616$nm, $\lambda_{ex} = 333$ nm, slits = 1.2-0.8).

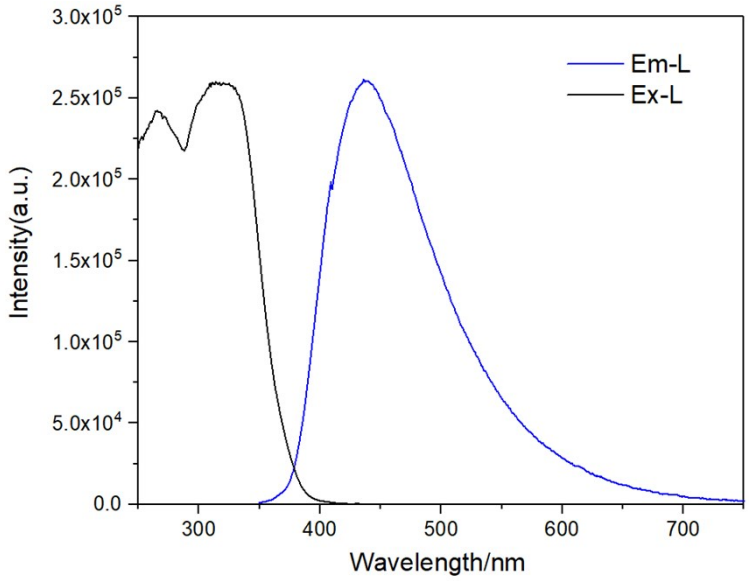

Figure S26. Excitation spectrum (black lines) and emission spectrum (blue lines) of L with equivalent Et_3N in H_2O (c = 2×10^{-5} M, λ_{em} = 438 nm, λ_{ex} = 324 nm, slits = 2.5-1.3).

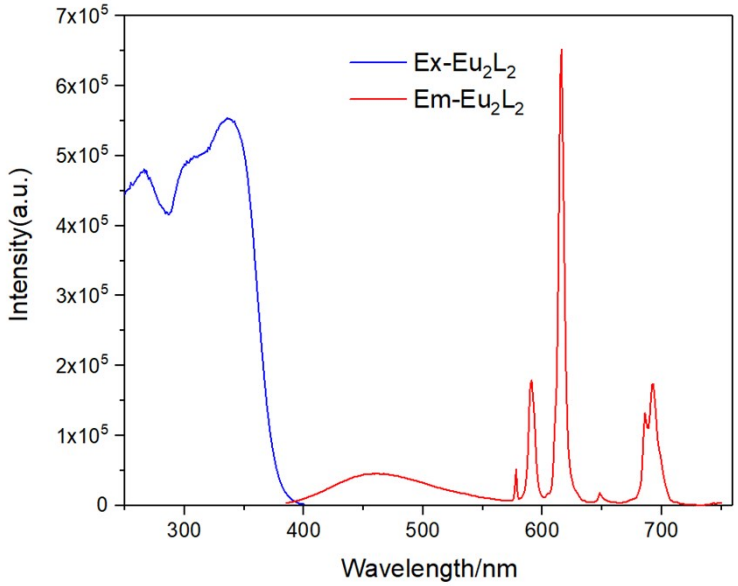

Figure S27. Excitation spectrum (blue lines) and emission spectrum (red lines) of Eu_2L_2 in H_2O (c=1×10^{-5} M, λ_{em} = 615nm, λ_{ex} = 336 nm, slits = 1.7-1.3).

3.2 Quantum yields

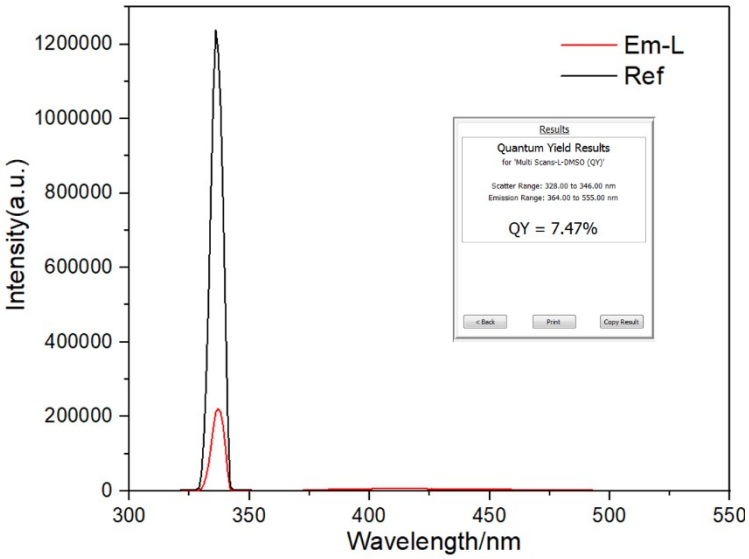

Figure S28. The superposition of emission spectra of reference and L with equivalent Et_3N ($\Phi_{overall}$ = 7.47%) (c = 2.00×10^{-5} M in DMSO; λ_{ex} = 334 nm, slits = 6.0-0.7).

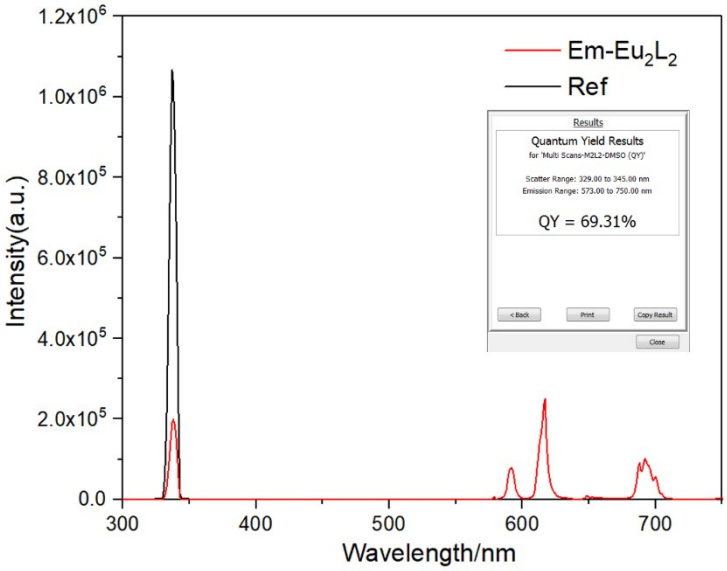

Figure S29. The superposition of emission spectra of reference and Eu_2L_2 ($\Phi_{overall}$ = 69.31%) (c = 1.00×10^{-5} M in DMSO; λ_{ex} = 333nm, slits = 6.0-0.65).

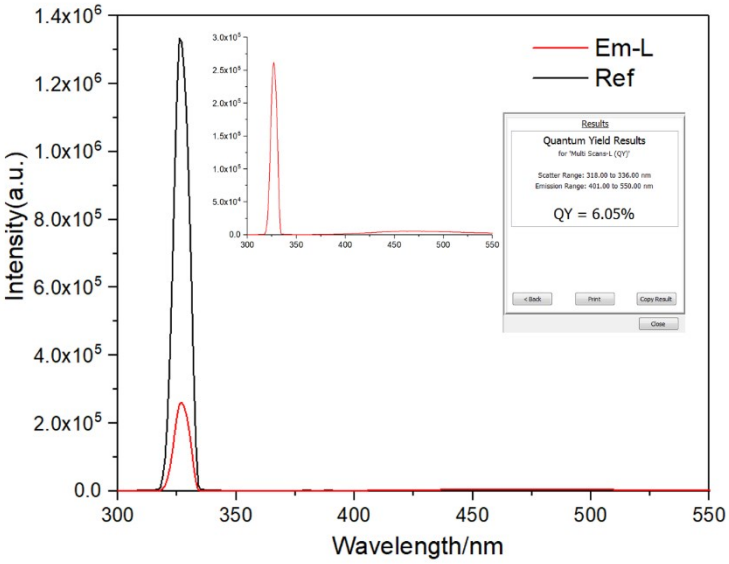

Figure S30. The superposition of emission spectra of reference and L with equivalent Et_3N ($\Phi_{overall}$ = 6.05%) (c = 2.00×10^{-5} M in H_2O; λ_{ex} = 324 nm, slits = 7.5-0.7).

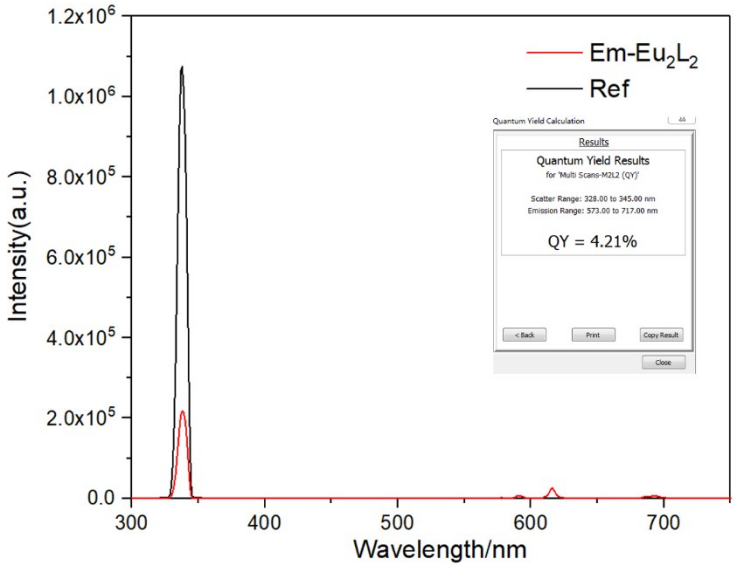

Figure S31. The superposition of emission spectra of reference and Eu_2L_2 ($\Phi_{overall}$ = 4.21%) (c = 1.00×10^{-5} M in H_2O; λ_{ex} = 336 nm, slits = 8.0-0.6).

3.3 Lifetime measurements

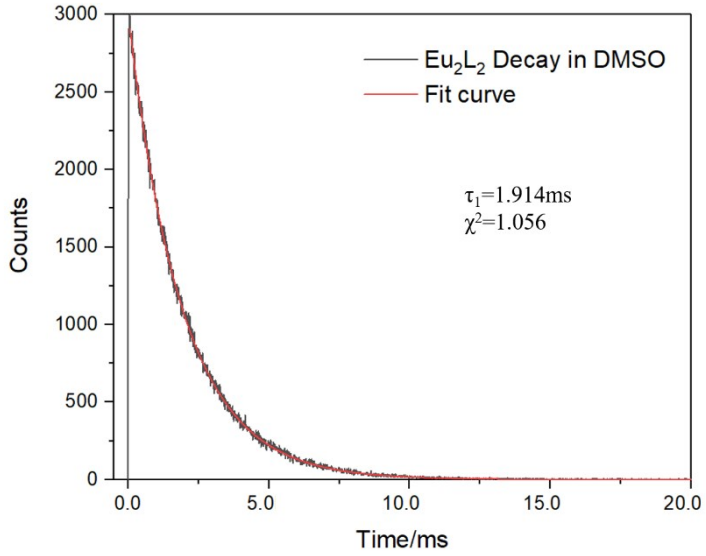

Figure S32. Excited state decay curve (black line) with mono exponential fit (red line) of Eu_2L_2 (c=1×10^{-5} M in DMSO, λ_{ex} = 333 nm, λ_{em} = 616 nm).

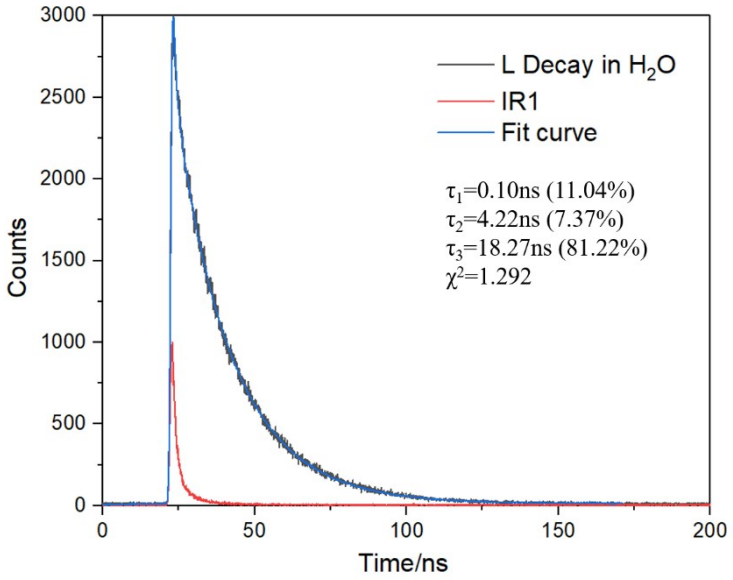

Figure S33. Excited state decay curve (black line), IR1(red line) and tri-exponential fit (blue line) of L with equivalent Et_3N (c=2×10^{-5} M in H_2O, λ_{ex} = 324 nm, λ_{em} = 438 nm).

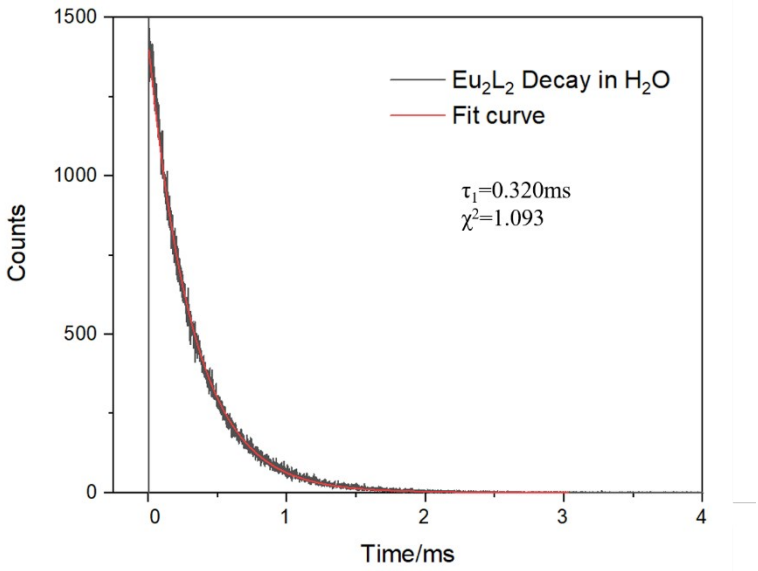

Figure S34. Excitated state decay curve (black line) with mono exponential fit (red line) of Eu_2L_2 (c=1×10^{-5} M in H_2O, λ_{ex} = 336 nm, λ_{em} = 615 nm).

3.4 Number of coordinated solvent molecules

Here, empirical equation is used to determine the number of solvent molecules q coordinated to Eu^{III} centers in compounds.

$$q=A\,(\tau_{water}^{-1} - \tau_{deutero\text{-}water}^{-1} - B) \qquad (1)$$

Where, empirically coefficients A = 1.05 and B = 0 were determined in H_2O and D_2O condition. [4] The calculated q values is 2.87 for **Eu_2L_2** in water.

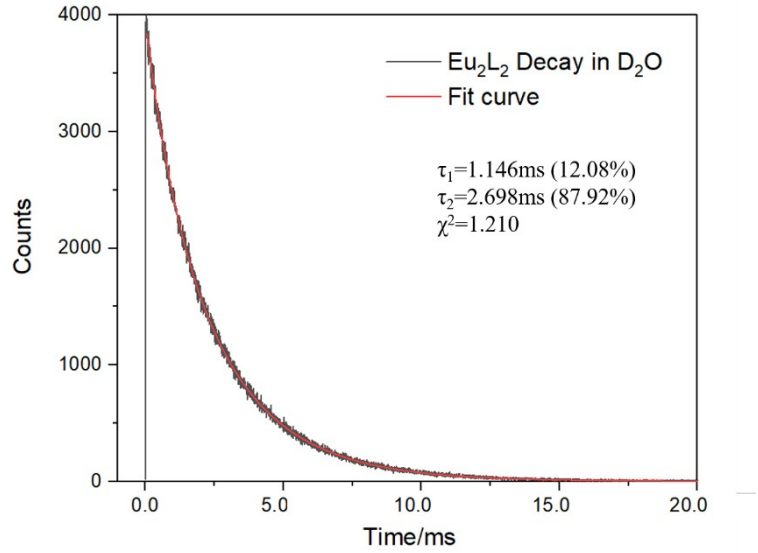

Figure S35. Excitated state decay curve (black line) with bi-exponential fit (red line) of Eu_2L_2 (c=1×10^{-5} M in D_2O, λ_{ex} = 336 nm, λ_{em} = 615 nm).

4 Chiral Sensing by PAM

4.1 Chiral optical measurements

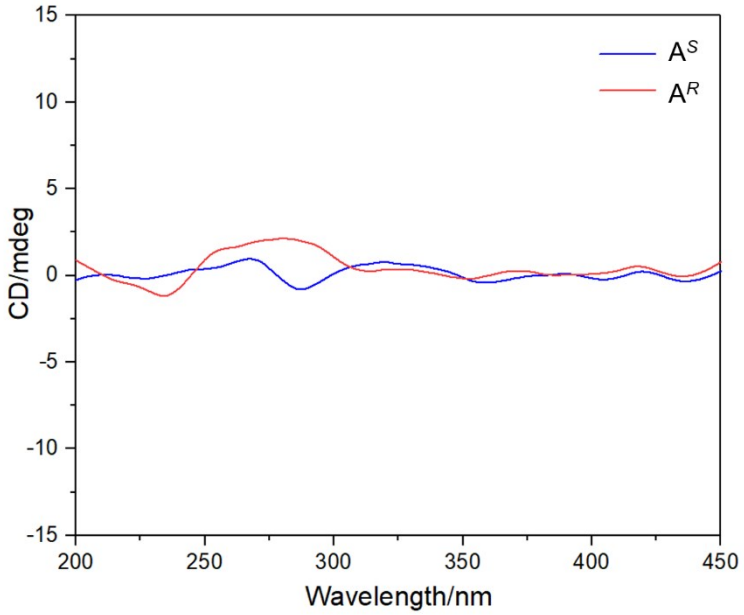

Figure S36. CD spectra of A^R and A^S (c = 1×10^{-5} M, CH_3CN).

4.2 UV-Vis absorption and Luminescence Spectra

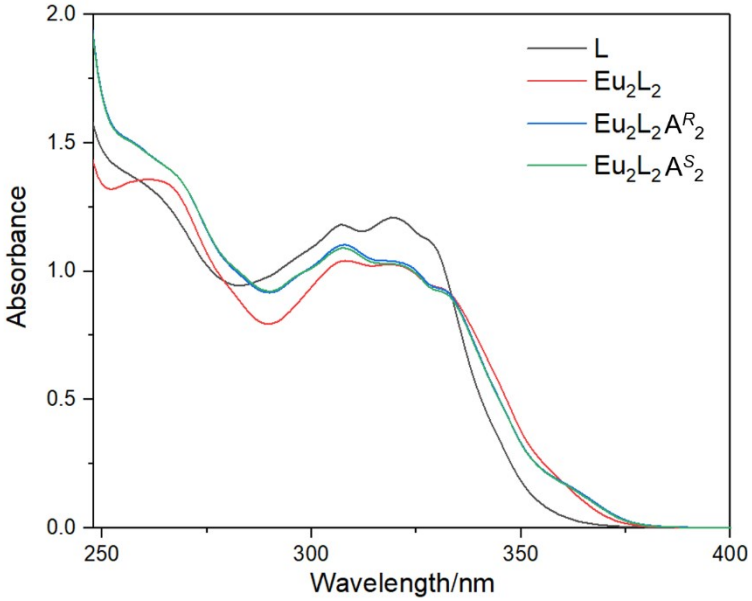

Figure S37. UV/Vis absorption spectra of L with equivalent Et_3N(c = 2.0×10^{-5} M), Eu_2L_2(c = 1.0×10^{-5} M), $Eu_2L_2A^R_2$(c = 1.0×10^{-5} M) and $Eu_2L_2A^S_2$(c = 1.0×10^{-5} M) in CH_3CN.

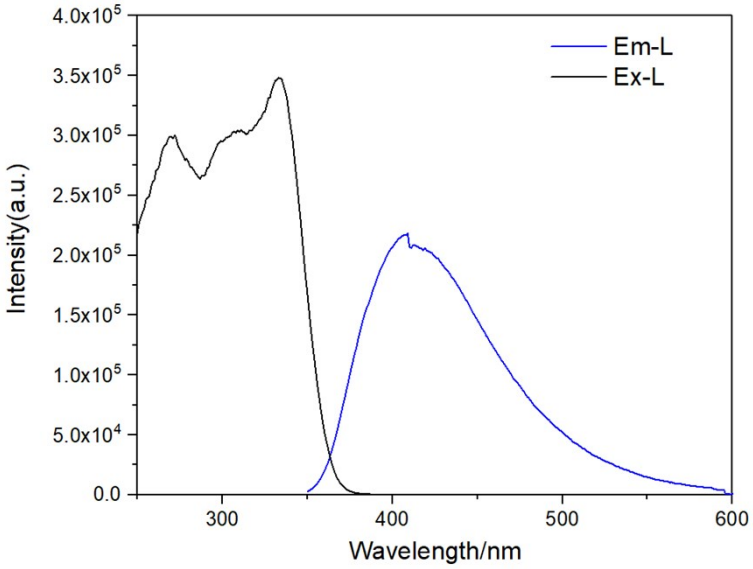

Figure S38. Excitation spectrum (black lines) and emission spectrum (blue lines) of L with equivalent Et_3N in CH_3CN ($c = 2\times10^{-5}$ M, λ_{em}= 406 nm, λ_{ex}= 333 nm, slits = 2.7-2).

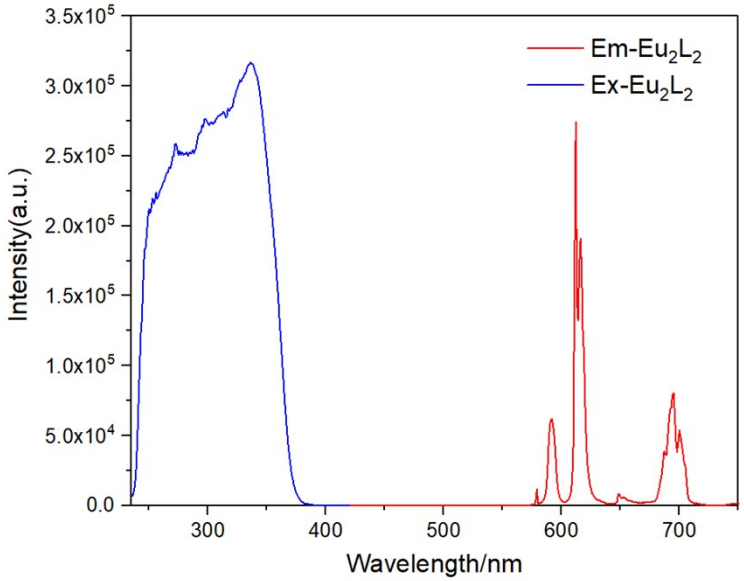

Figure S39. Excitation spectrum (blue lines) and emission spectrum (red lines) of Eu_2L_2 in CH_3CN ($c = 1\times10^{-5}$ M, λ_{em} = 612 nm, λ_{ex} = 335 nm, slits = 1.2-0.5).

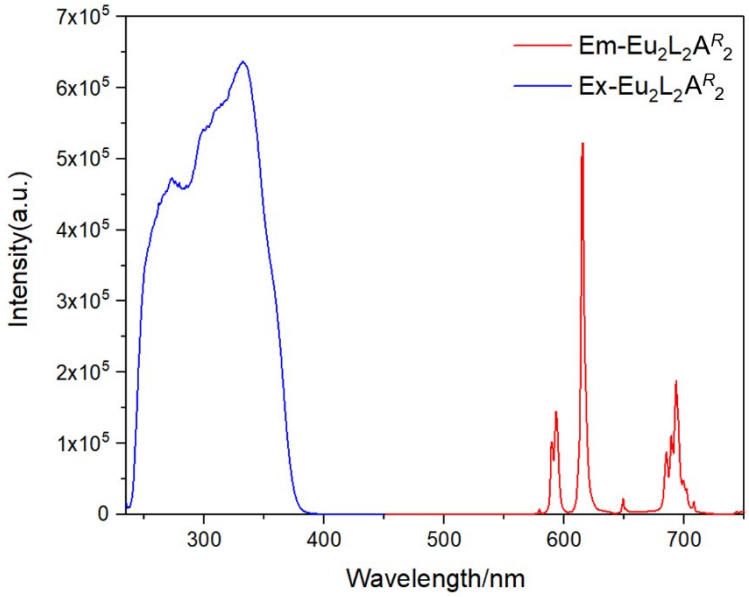

Figure S40. Excitation spectrum (blue lines) and emission spectrum (red lines) of $Eu_2L_2A^R_2$ in CH_3CN (c = 1×10^{-5} M, λ_{em} = 615nm, λ_{ex} = 335 nm, slits = 1.2-0.5).

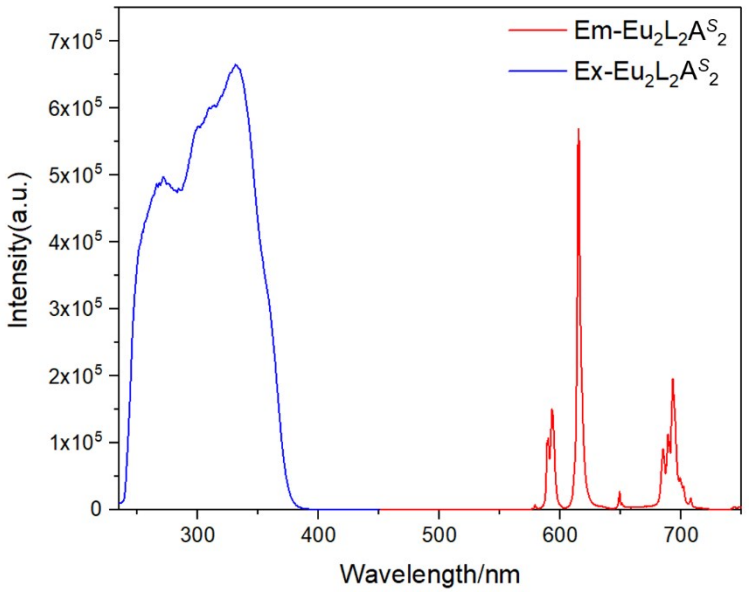

Figure S41. Excitation spectrum (blue lines) and emission spectrum (red lines) of $Eu_2L_2A^S_2$ in CH_3CN (*c* = 1×10^{-5} M, λ_{em} = 615nm, λ_{ex} = 335 nm, slits = 1.2-0.5).

4.3 Quantum yields

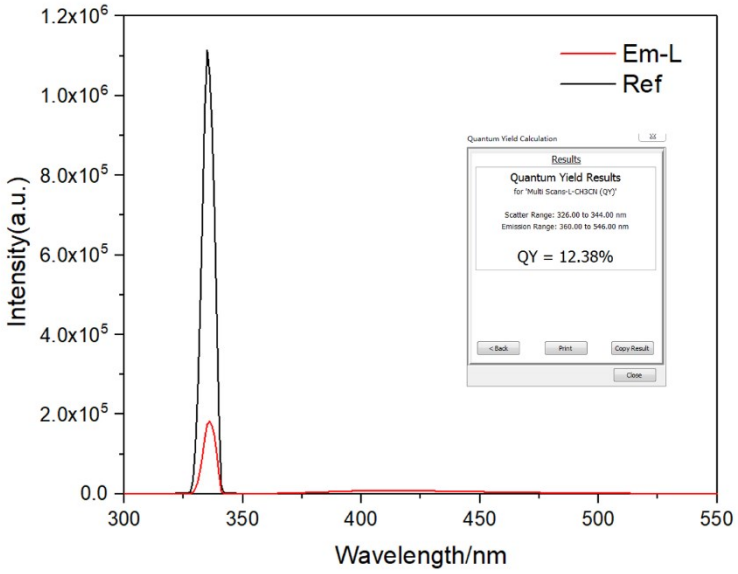

Figure S42. The superposition of emission spectra of reference and L with equivalent Et_3N ($\Phi_{overall}$ = 12.38%) (c = 2.00×10^{-5} M in CH_3CN; λ_{ex} = 333 nm, slits = 6.0-0.65).

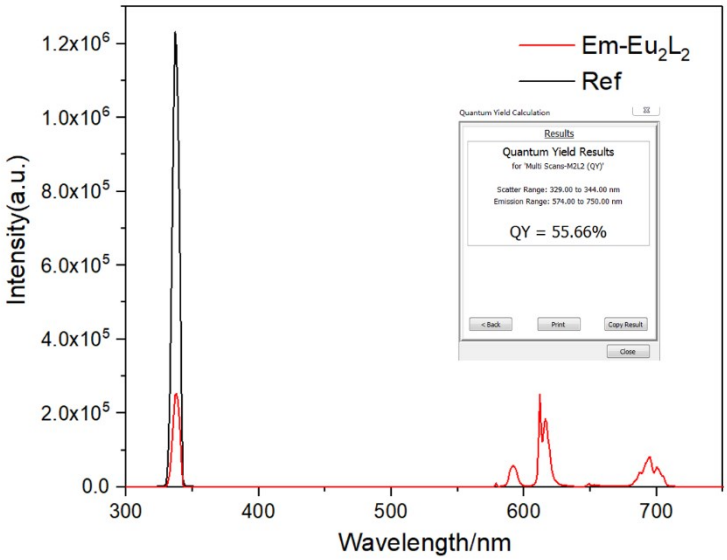

Figure S43. The superposition of emission spectra of reference and Eu_2L_2 ($\Phi_{overall}$ = 55.66%) (c = 1.00×10^{-5} M in CH_3CN; λ_{ex} = 335 nm, slits = 6.0-0.7).

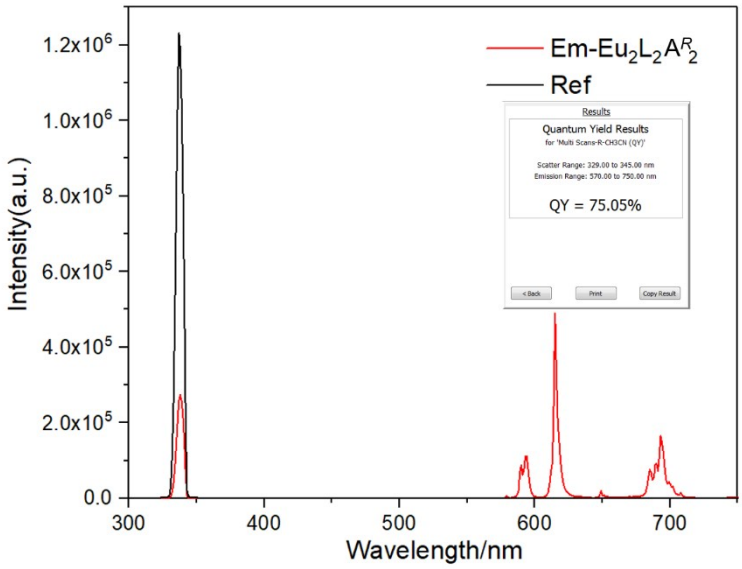

Figure S44. The superposition of emission spectra of reference and $Eu_2L_2A^R_2$ ($\Phi_{overall}$ = 75.05 %) (c = 1.00×10^{-5} M in CH_3CN; λ_{ex} = 335 nm, slits = 6.0-0.7).

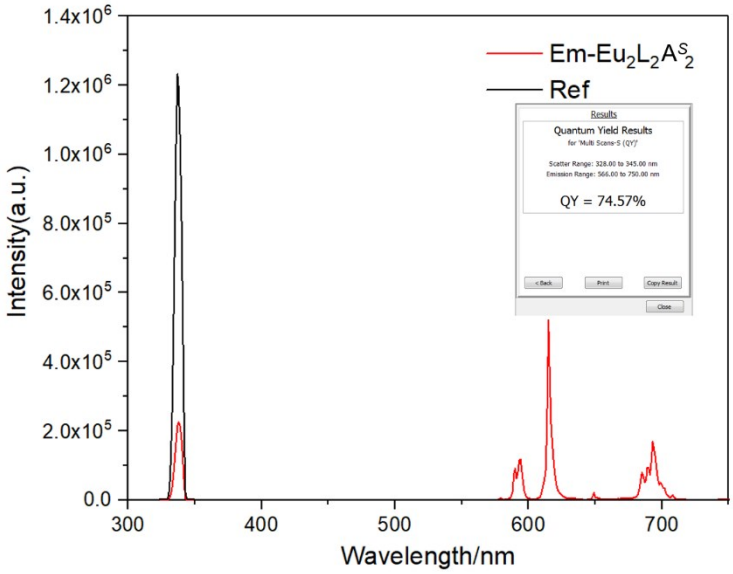

Figure S45. The superposition of emission spectra of reference and $Eu_2L_2A^S_2$ ($\Phi_{overall}$ = 74.57%) (c = 1.00×10^{-5} M in CH_3CN; λ_{ex} = 335 nm, slits = 6.0-0.7).

4.4 Lifetime measurements

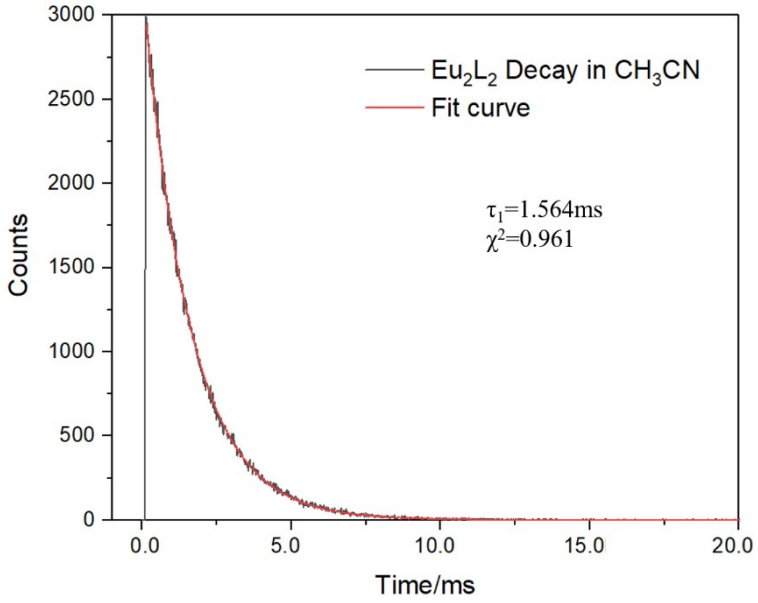

Figure S46. Excited state decay curve (black line) with mono exponential fit (red line) of Eu_2L_2 (c = 1×10^{-5} M in CH_3CN, λ_{ex} = 335 nm, λ_{em} = 612 nm).

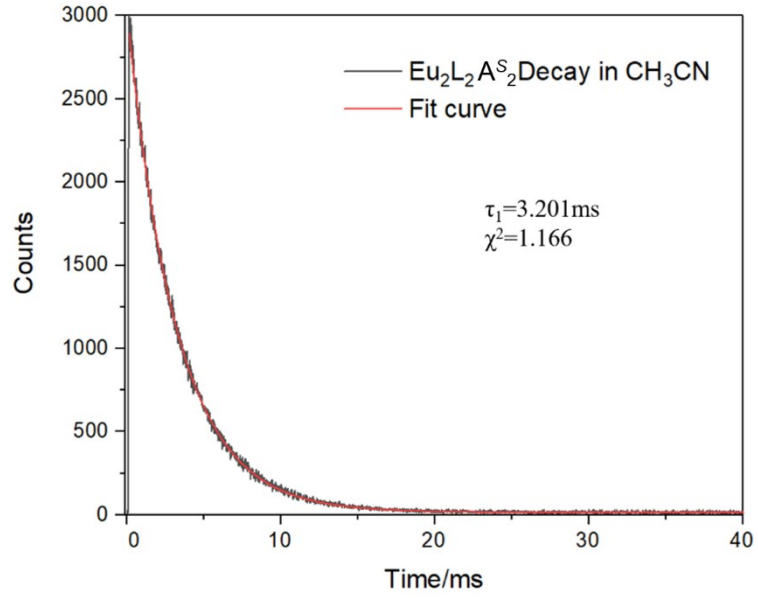

Figure S47. Excited state decay curve (black line) with mono exponential fit (red line) of $Eu_2L_2A^S_2$ (c = 1×10^{-5} M in CH_3CN, λ_{ex} = 335 nm, λ_{em} = 615 nm).

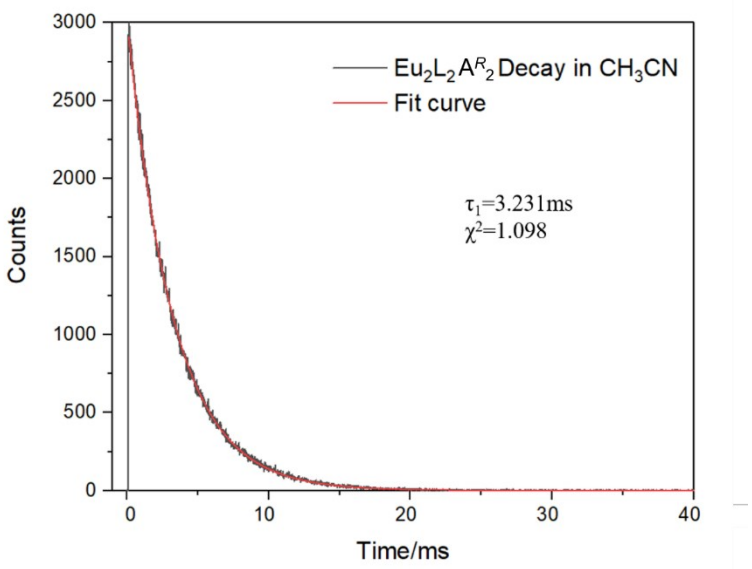

Figure S48. Excitated state decay curve (black line) with mono exponential fit (red line) of $Eu_2L_2A^R_2$ (c = 1×10^{-5} M in CH_3CN, λ_{ex} = 335 nm, λ_{em} = 615 nm).

5 Pesticide Detection by disassembly

5.1 UV-Vis absorption and Luminescence Spectra

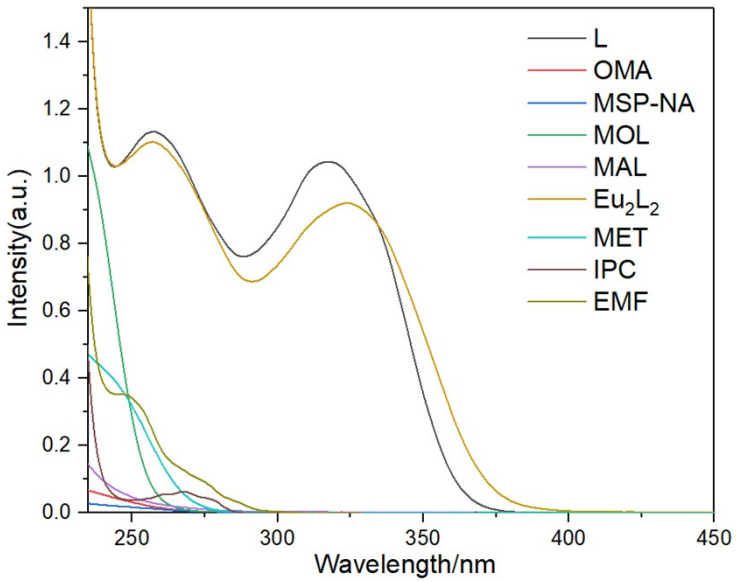

Figure S49. UV/Vis absorption spectra of L with equivalent Et_3N(c = 2.0×10^{-5} M), Eu_2L_2(c = 1.0×10^{-5} M), OMA(c = 1.0×10^{-4} M), MSP-Na(c = 1.0×10^{-4} M), MOL(c = 1.0×10^{-4} M), MAL(c = 1.0×10^{-4} M),MET(c = 1.0×10^{-4} M), IPC(c = 1.0×10^{-4} M) and EMF(c = 1.0×10^{-4} M) in H_2O.

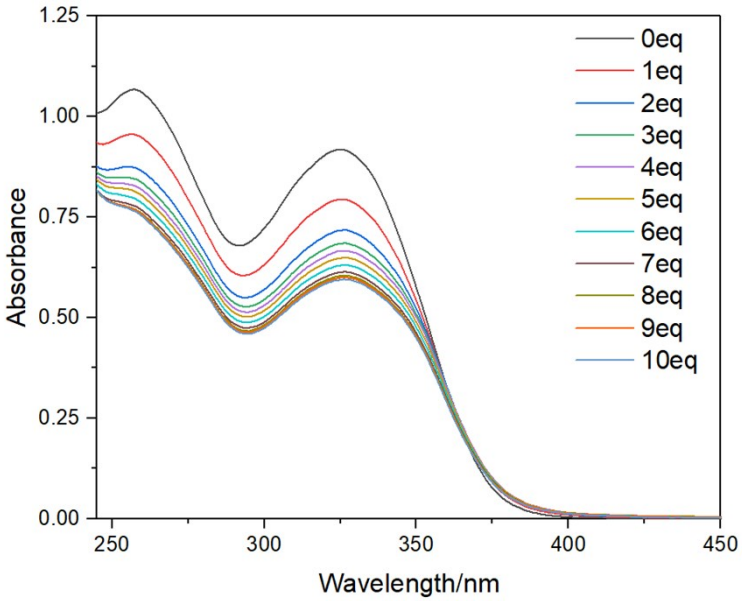

Figure S50. UV titration spectra of Eu_2L_2 in H_2O (c = 1×10^{-5} M) upon addition of different equiv of MAL.

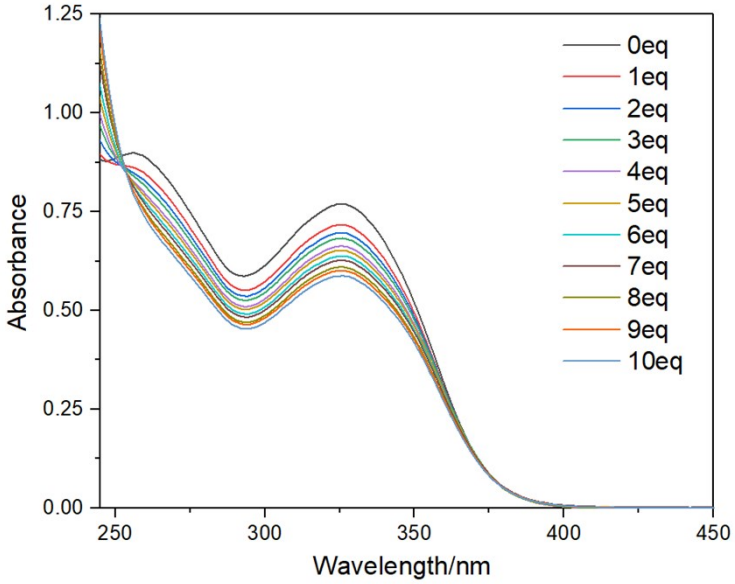

Figure S51. UV titration spectra of Eu_2L_2 in H_2O (c = 1×10^{-5} M) upon addition of different equiv of MOL.

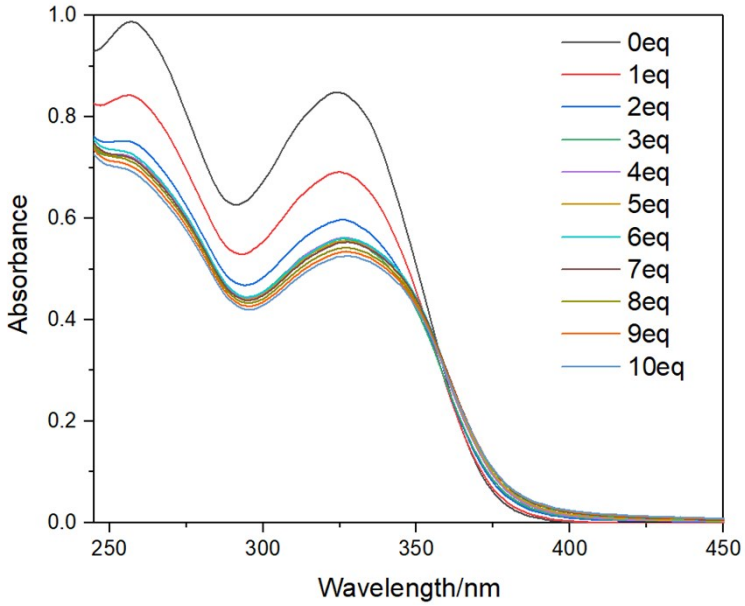

Figure S52. UV titration spectra of Eu_2L_2 in H_2O (c = 1×10^{-5} M) upon addition of different equiv of MSP-Na.

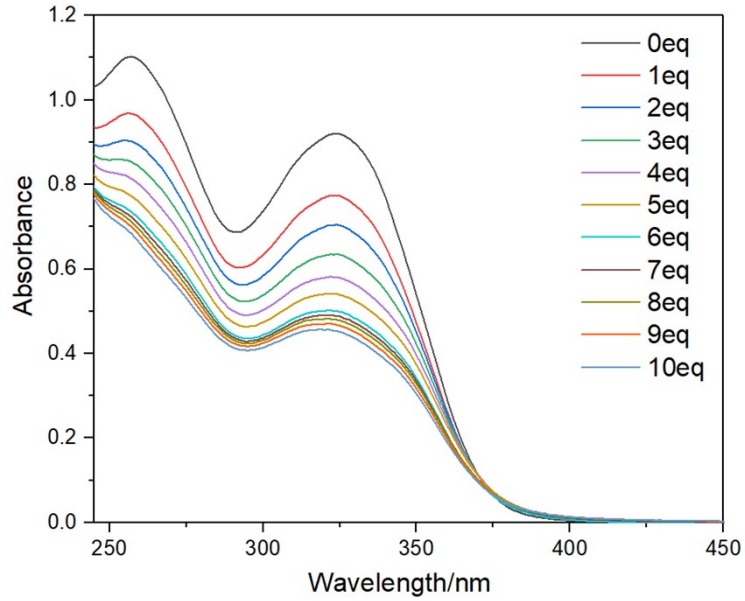

Figure S53. UV titration spectra of Eu_2L_2 in H_2O (c = 1×10^{-5} M) upon addition of different equiv of OMA.

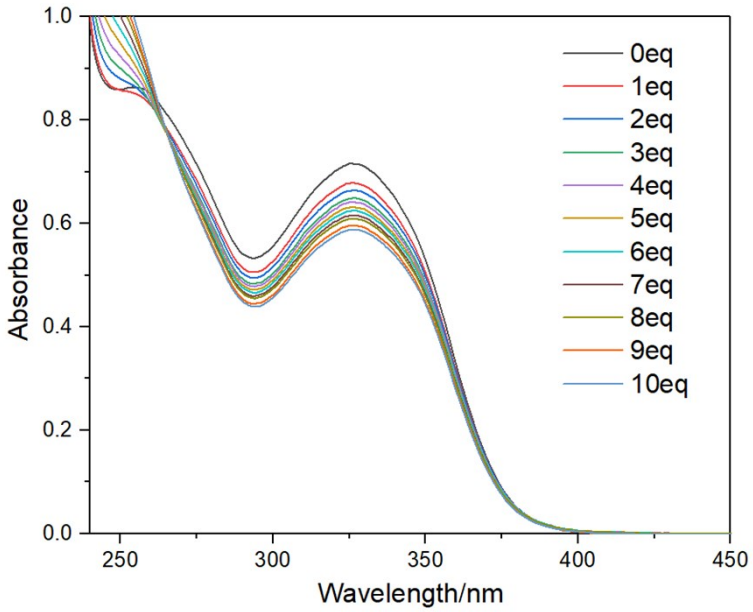

Figure S54. UV titration spectra of Eu_2L_2 in H_2O (c = 1×10^{-5} M) upon addition of different equiv of MET.

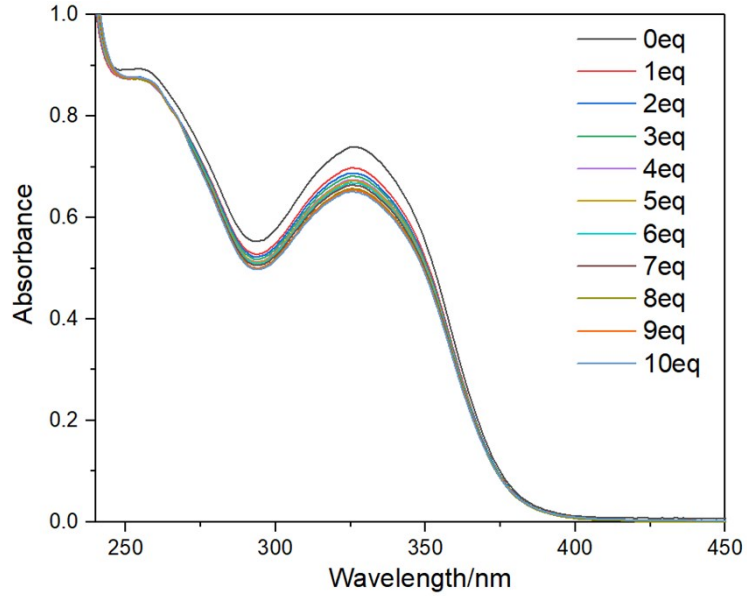

Figure S55. UV titration spectra of Eu_2L_2 in H_2O (c=1×10^{-5} M) upon addition of different equiv of IPC.

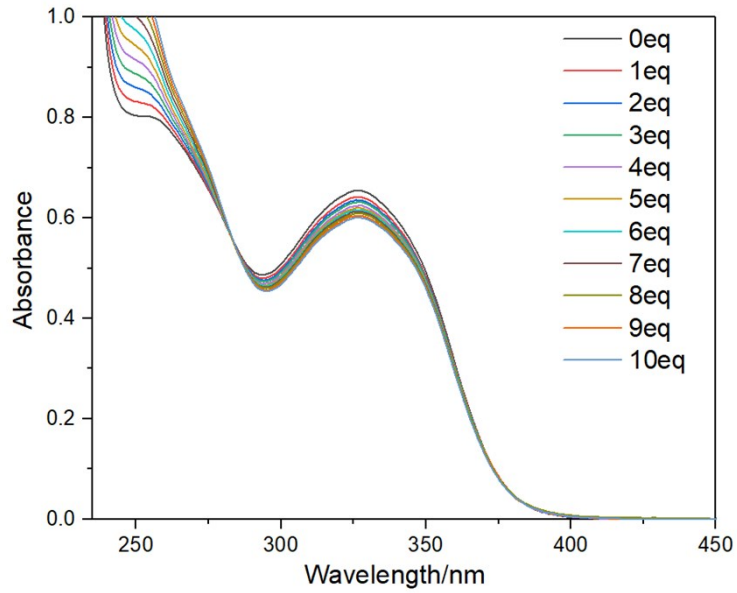

Figure S56. UV titration spectra of Eu_2L_2 in H_2O (c = 1×10^{-5} M) upon addition of different equiv of EMF.

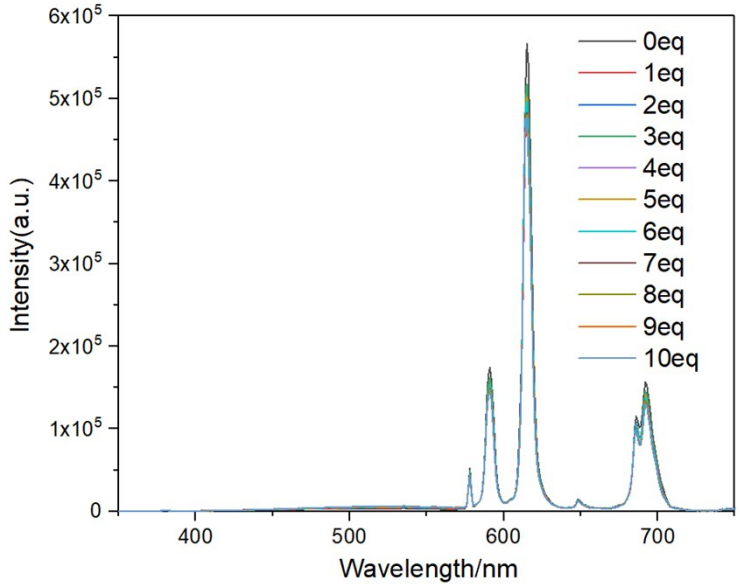

Figure S57. Fluorescent titration spectra of Eu_2L_2 in H_2O (c = 1×10^{-5} M) upon addition of different equiv of MAL.

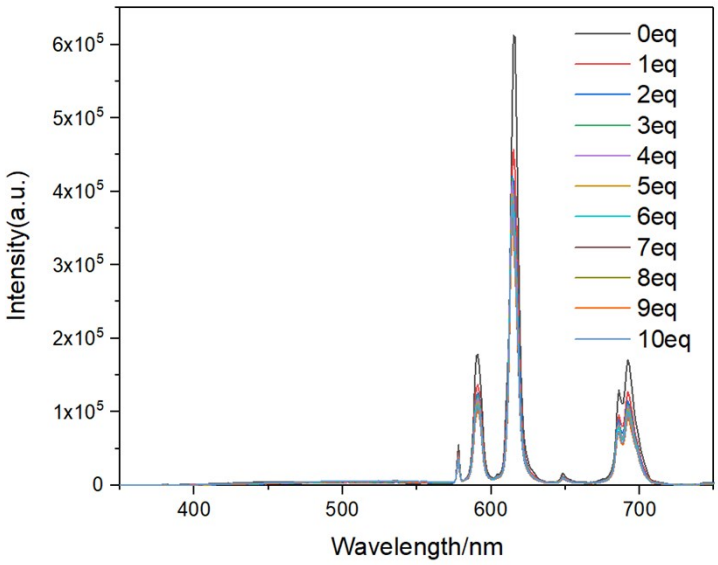

Figure S58. Fluorescent titration spectra of Eu_2L_2 in H_2O (c = 1×10^{-5} M) upon addition of different equiv of MOL.

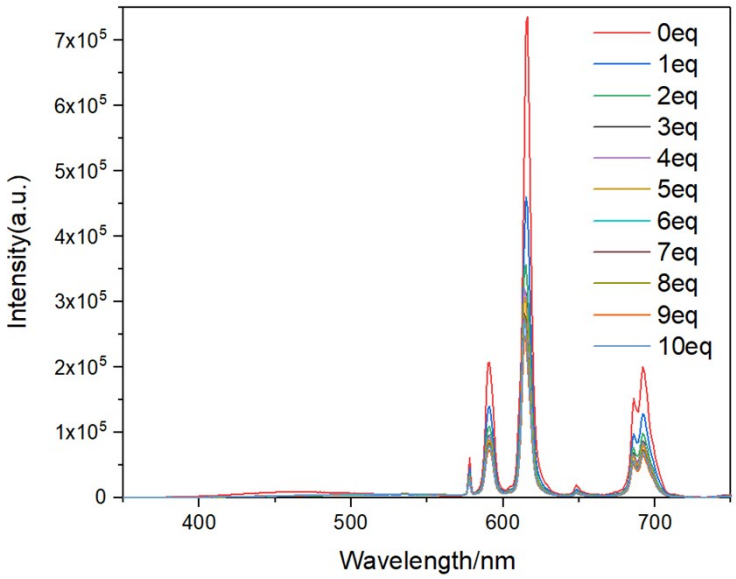

Figure S59. Fluorescent titration spectra of Eu_2L_2 in H_2O (c = 1×10^{-5} M) upon addition of different equiv of MSP-Na.

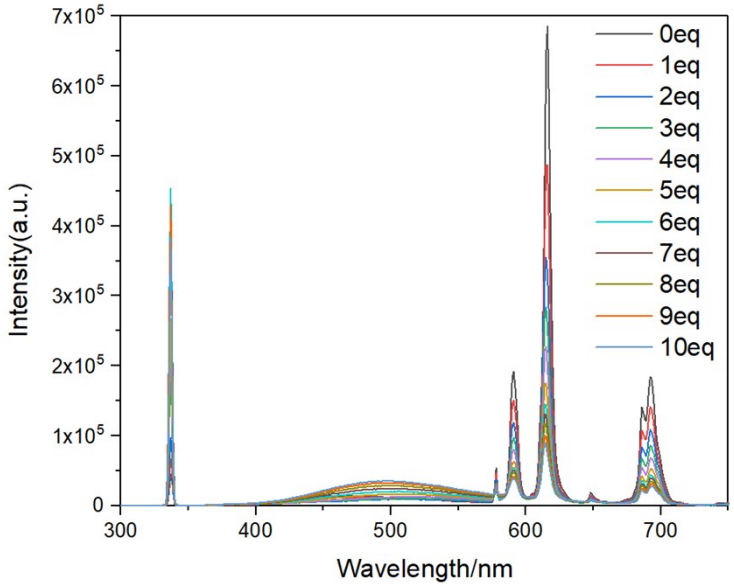

Figure S60. Fluorescent titration spectra of Eu_2L_2 in H_2O (c = 1×10^{-5} M) upon addition of different equiv of OMA.

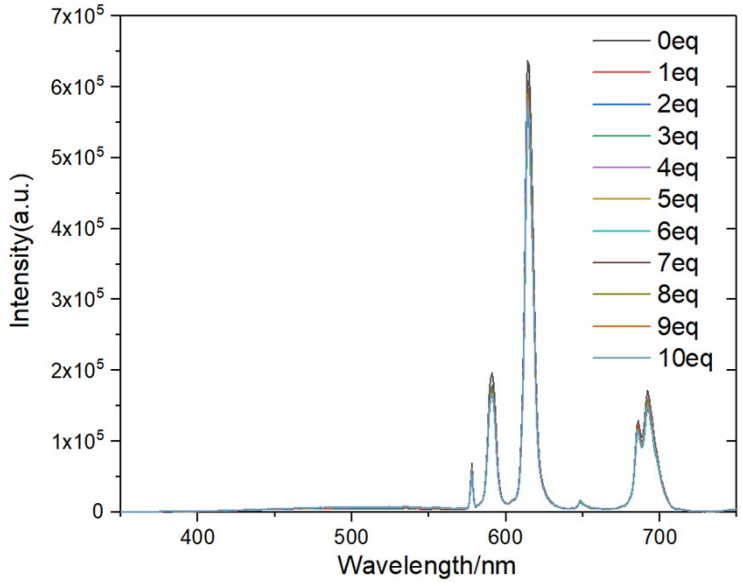

Figure S61. Fluorescent titration spectra of Eu_2L_2 in H_2O (c = 1×10^{-5} M) upon addition of different equiv of MET.

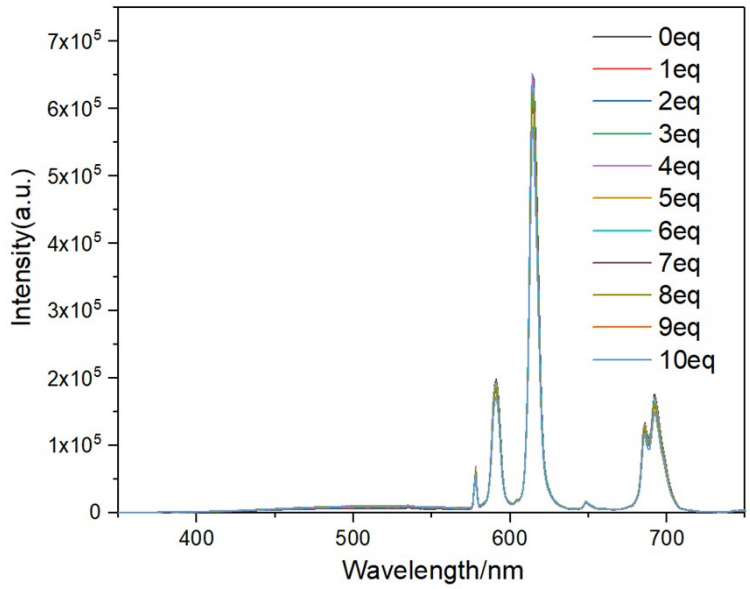

Figure S62. Fluorescent titration spectra of Eu_2L_2 in H_2O (c = 1×10^{-5} M) upon addition of different equiv of IPC.

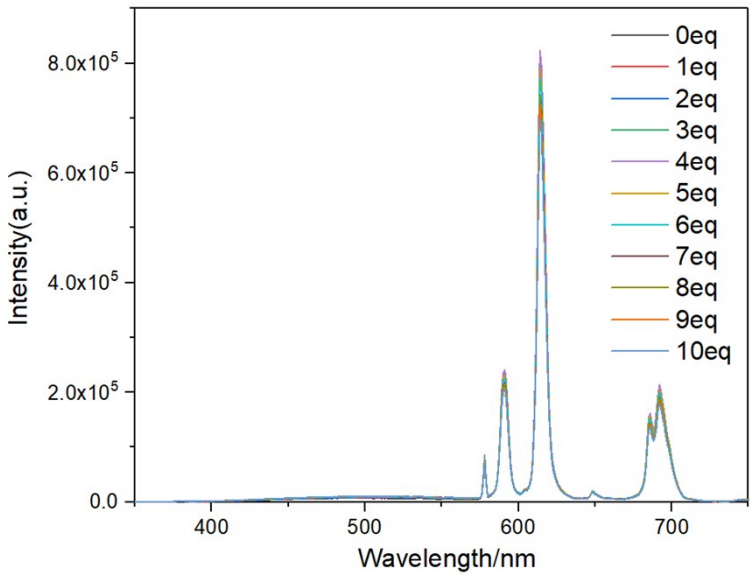

Figure S63. Fluorescent titration spectra of Eu_2L_2 in H_2O (c = 1×10^{-5} M) upon addition of different equiv of EMF.

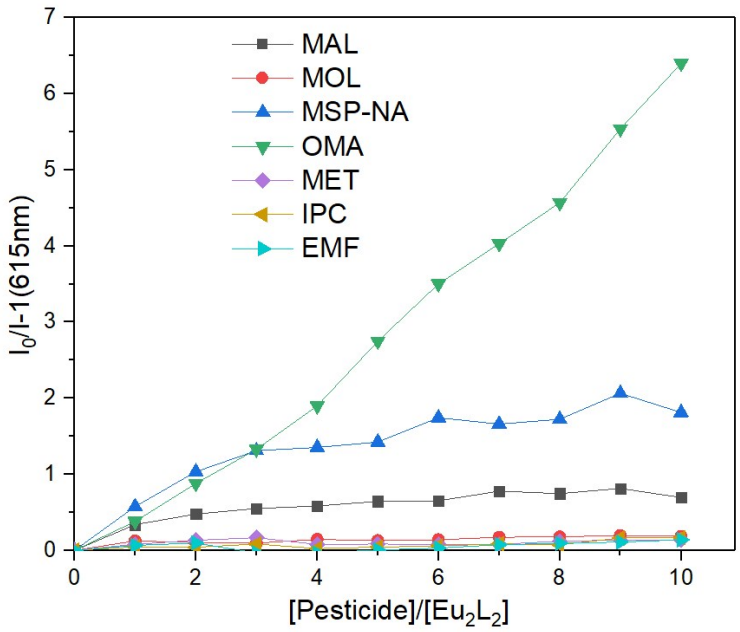

Figure S64. Fluorescence emission changes of Eu_2L_2 at 615nm when different pesticides were added.

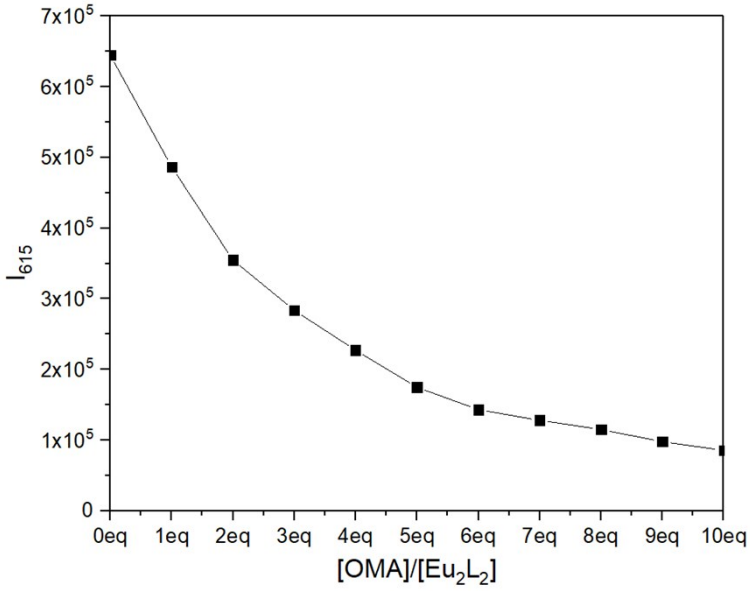

Figure S65. Fluorescence emission changes of Eu_2L_2 at 615nm when different equivalents of OMA are added.

5.2 Quantum yields

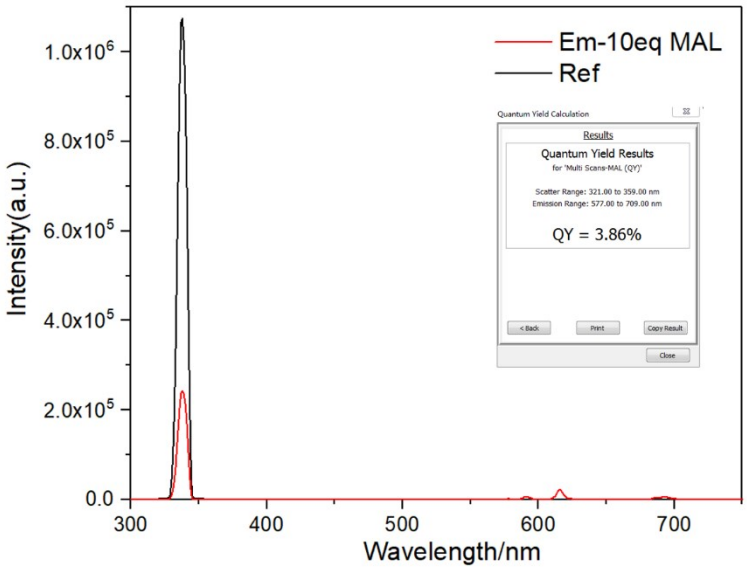

Figure S66. The superposition of emission spectra of reference and Eu_2L_2 with 10 equiv MAL ($\Phi_{overall}$ = 3.86%) (c = 1.00×10^{-5} M in H_2O; λ_{ex} = 336 nm, slits = 8.0-0.6).

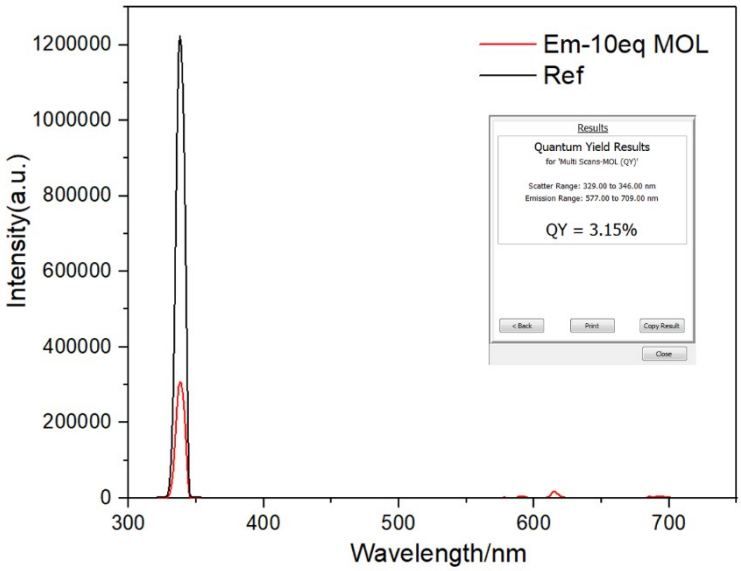

Figure S67. The superposition of emission spectra of reference and Eu_2L_2 with 10 equiv MOL ($\Phi_{overall}$ = 3.15%) (c = 1.00×10^{-5} M in H_2O; λ_{ex} = 336 nm, slits = 8.0-0.7).

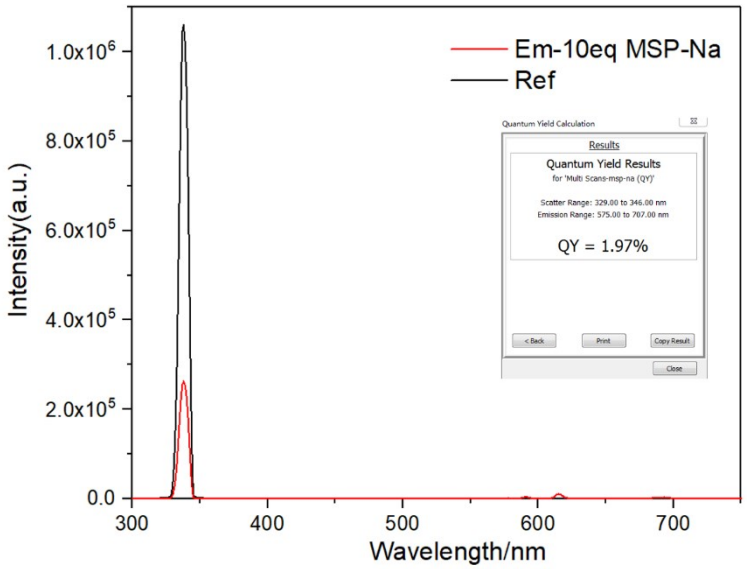

Figure S68. The superposition of emission spectra of reference and Eu_2L_2 with 10 equiv MSP-Na ($\Phi_{overall}$ = 1.97%) (c = 1.00×10^{-5} M in H_2O; λ_{ex} = 336 nm, slits = 8.0-0.6).

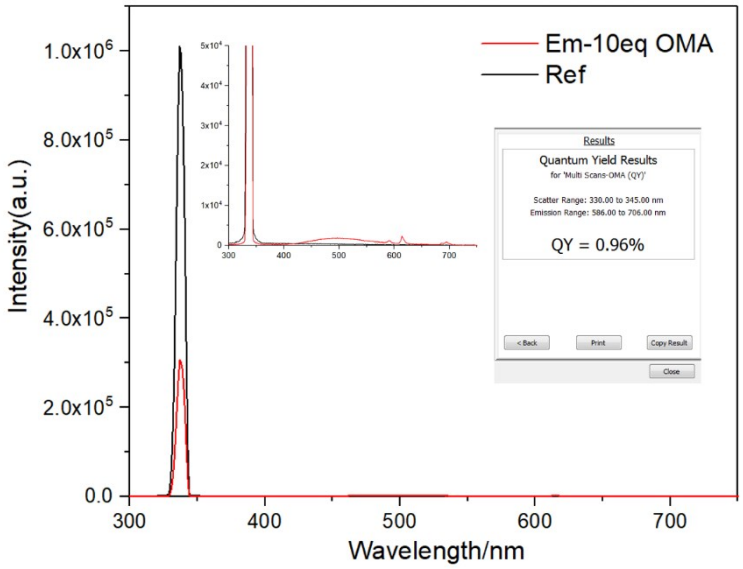

Figure S69. The superposition of emission spectra of reference and Eu_2L_2 with 10 equiv OMA ($\Phi_{overall}$ = 0.96%) (c = 1.00×10^{-5} M in H_2O; λ_{ex} = 336 nm, slits = 7.0-0.6).

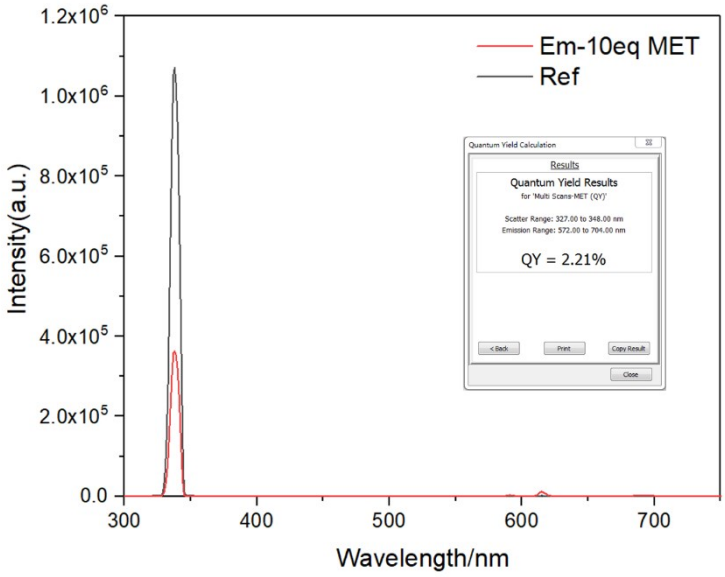

Figure S70. The superposition of emission spectra of reference and Eu_2L_2 with 10 equiv MET ($\Phi_{overall}$ = 2.21%) (c = 1.00×10^{-5} M in H_2O; λ_{ex} = 336 nm, slits = 8.0-0.65).

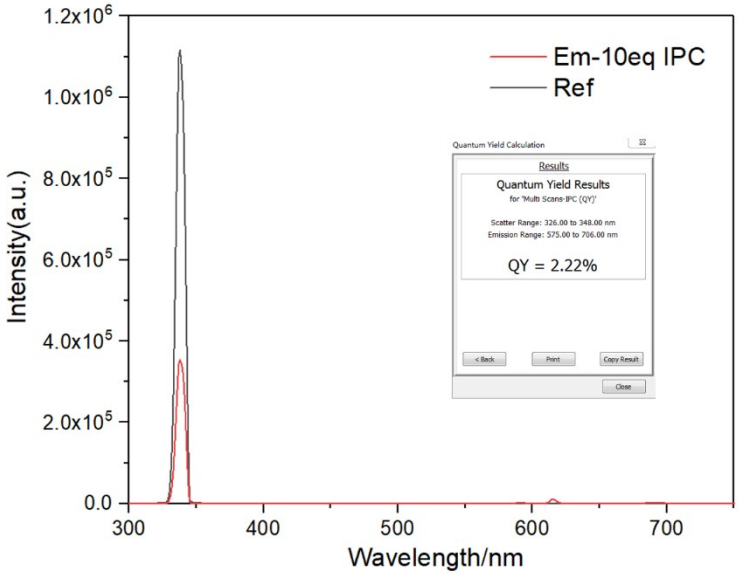

Figure S71. The superposition of emission spectra of reference and Eu_2L_2 with 10 equiv IPC ($\Phi_{overall}$ = 2.22%) (c = 1.00×10^{-5} M in H_2O; λ_{ex} = 336 nm, slits = 8.0-0.65).

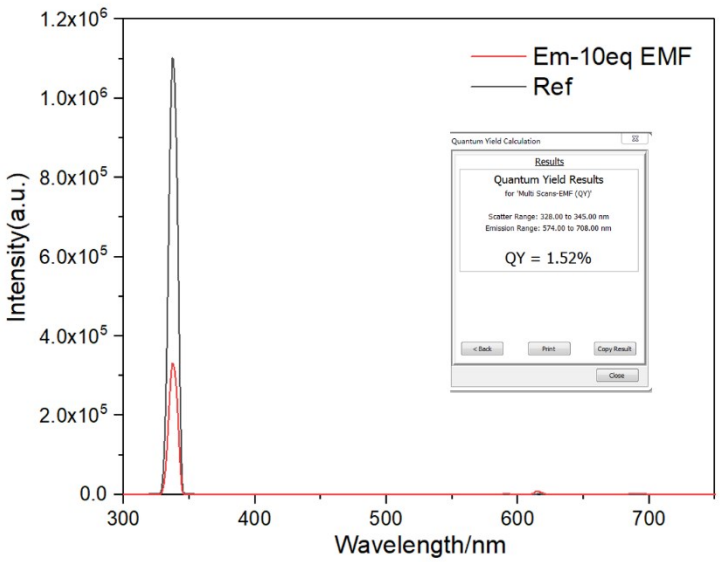

Figure S72. The superposition of emission spectra of reference and Eu_2L_2 with 10 equiv EMF ($\Phi_{overall}$ = 1.52%) (c = 1.00×10^{-5} M in H_2O; λ_{ex} = 336 nm, slits = 8.0-0.6).

6 Mass spectra

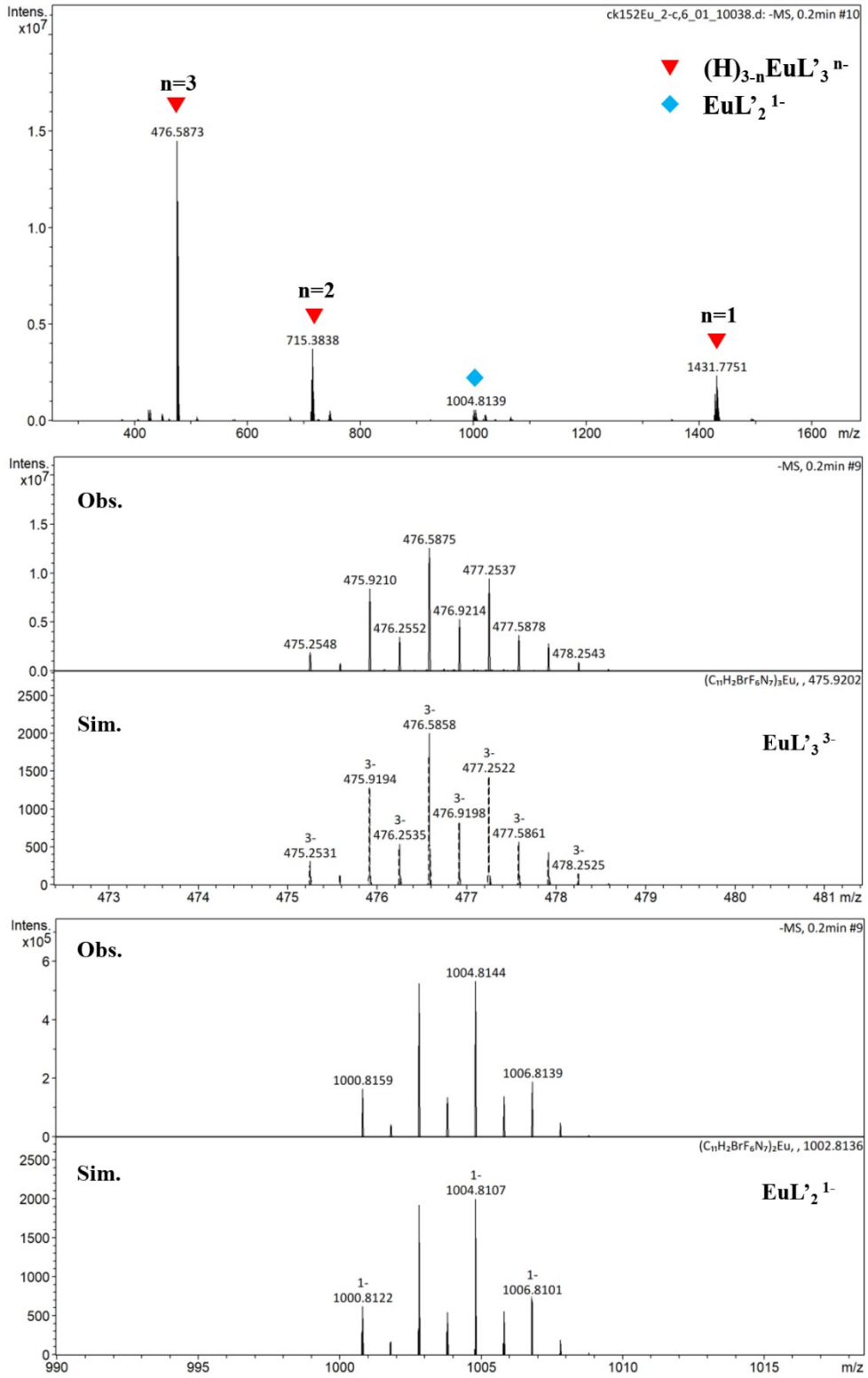

Figure S73. ESI-TOF-MS spectra for EuL'_3 and EuL'_2 in CH_3CN with insets showing the observed and calculated isotopic patterns of the peaks.

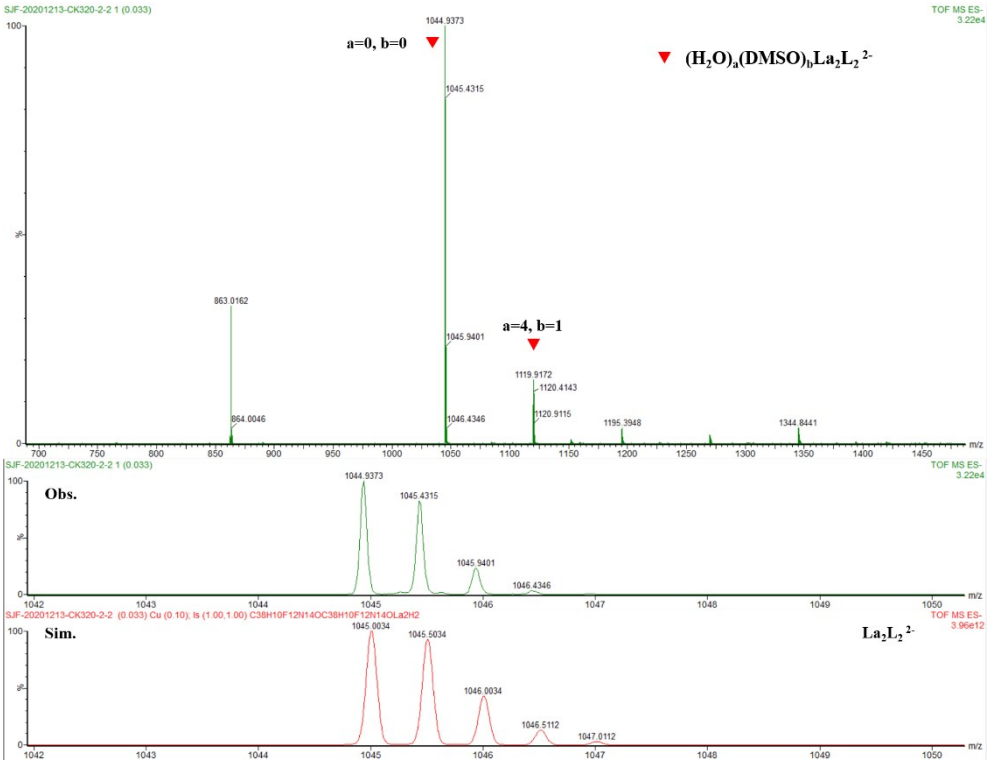

Figure S74. ESI-MS spectrum for La_2L_2 in DMSO with insets showing the observed and calculated isotopic patterns of the peaks.

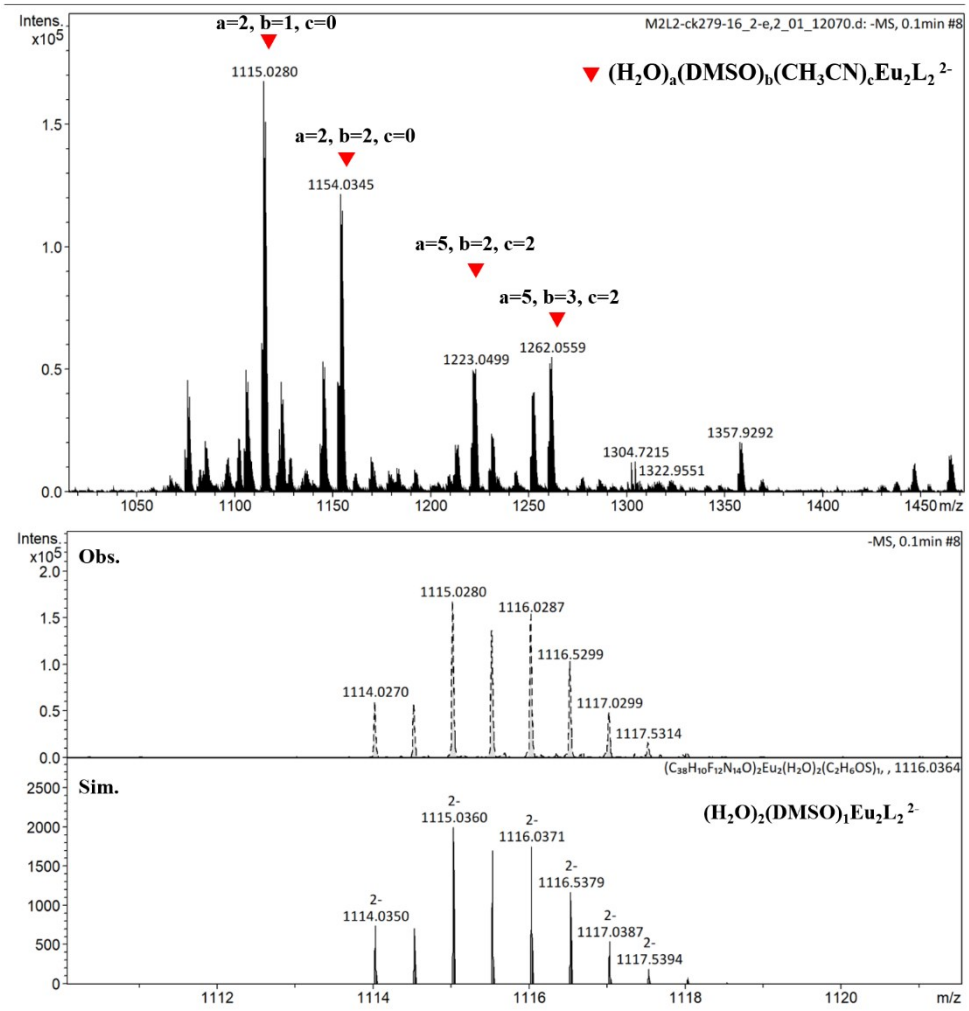

Figure S75. ESI-TOF-MS spectrum for Eu_2L_2 in DMSO with insets showing the observed and calculated isotopic patterns of the peak.

Table S1. Comparison of the observed and simulated signals in the ESI-TOF-MS spectrum of Eu_2L_2.

Valence	Molecular formula	Observed	Simulated
-2	$(C_{38}H_{10}F_{12}N_{14}O)_2Eu_2(H_2O)_2(C_2H_6OS)_1$	1115.0279	1115.0360
-2	$(C_{38}H_{10}F_{12}N_{14}O)_2Eu_2(H_2O)_3(C_2H_6OS)_1$	1124.0324	1124.0412
-2	$(C_{38}H_{10}F_{12}N_{14}O)_2Eu_2(H_2O)_2(C_2H_6OS)_2$	1154.0344	1154.0429
-2	$(C_{38}H_{10}F_{12}N_{14}O)_2Eu_2(H_2O)_4(C_2H_6OS)_2$ $(CH_3CN)_2$	1213.0439	1213.0800
-2	$(C_{38}H_{10}F_{12}N_{14}O)_2Eu_2(H_2O)_5(C_2H_6OS)_2$ $(CH_3CN)_2$	1222.0486	1222.0853
-2	$(C_{38}H_{10}F_{12}N_{14}O)_2Eu_2(H_2O)_6(C_2H_6OS)_2$ $(CH_3CN)_2$	1231.0538	1231.0906
-2	$(C_{38}H_{10}F_{12}N_{14}O)_2Eu_2(H_2O)_4(C_2H_6OS)_3$ $(CH_3CN)_2$	1253.0522	1253.0880
-2	$(C_{38}H_{10}F_{12}N_{14}O)_2Eu_2(H_2O)_5(C_2H_6OS)_3$ $(CH_3CN)_2$	1262.0565	1262.0933

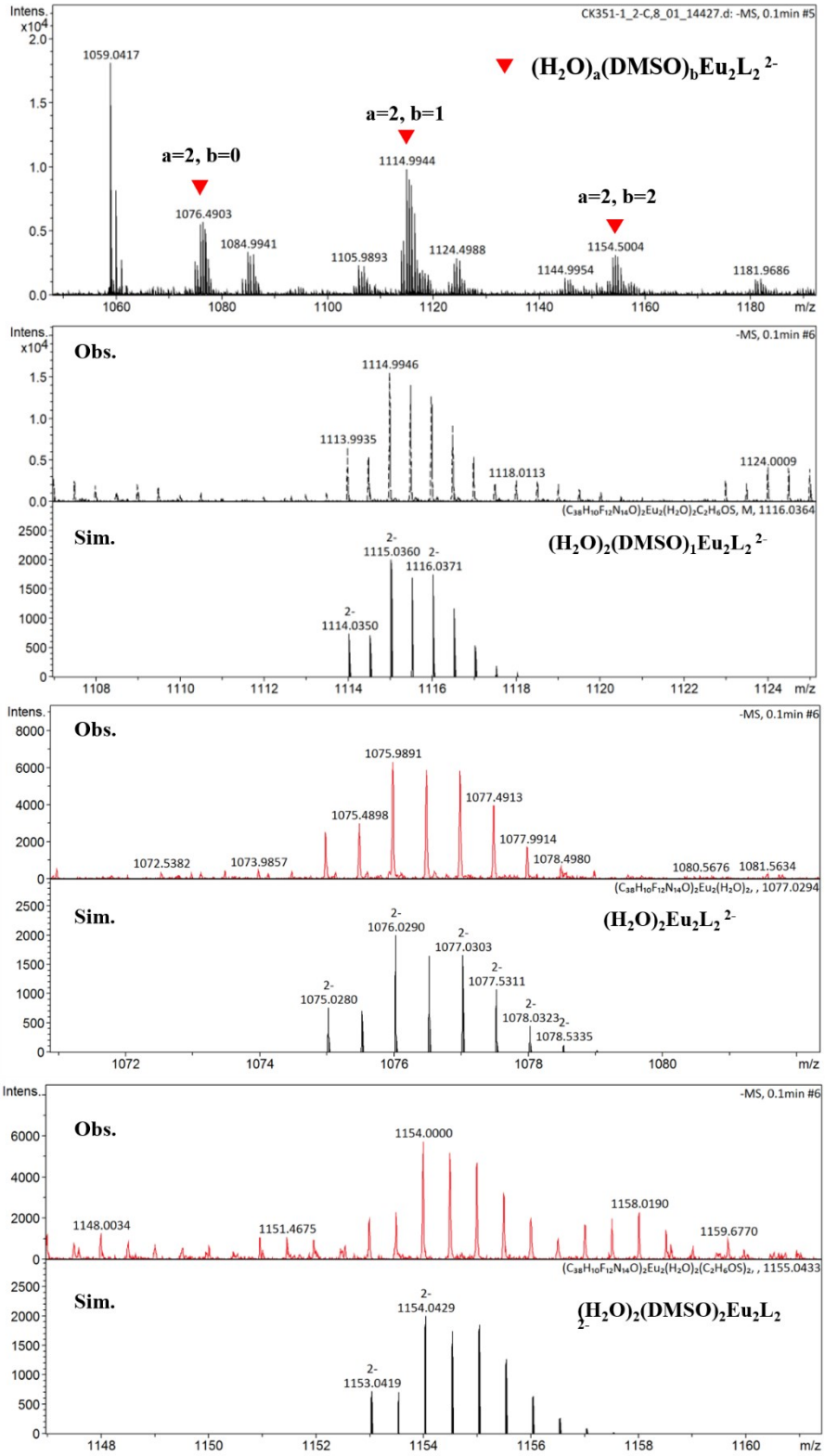

Figure S76. ESI-TOF-MS spectrum for Eu_2L_2 in H_2O with insets showing the observed and calculated isotopic patterns of the peaks.

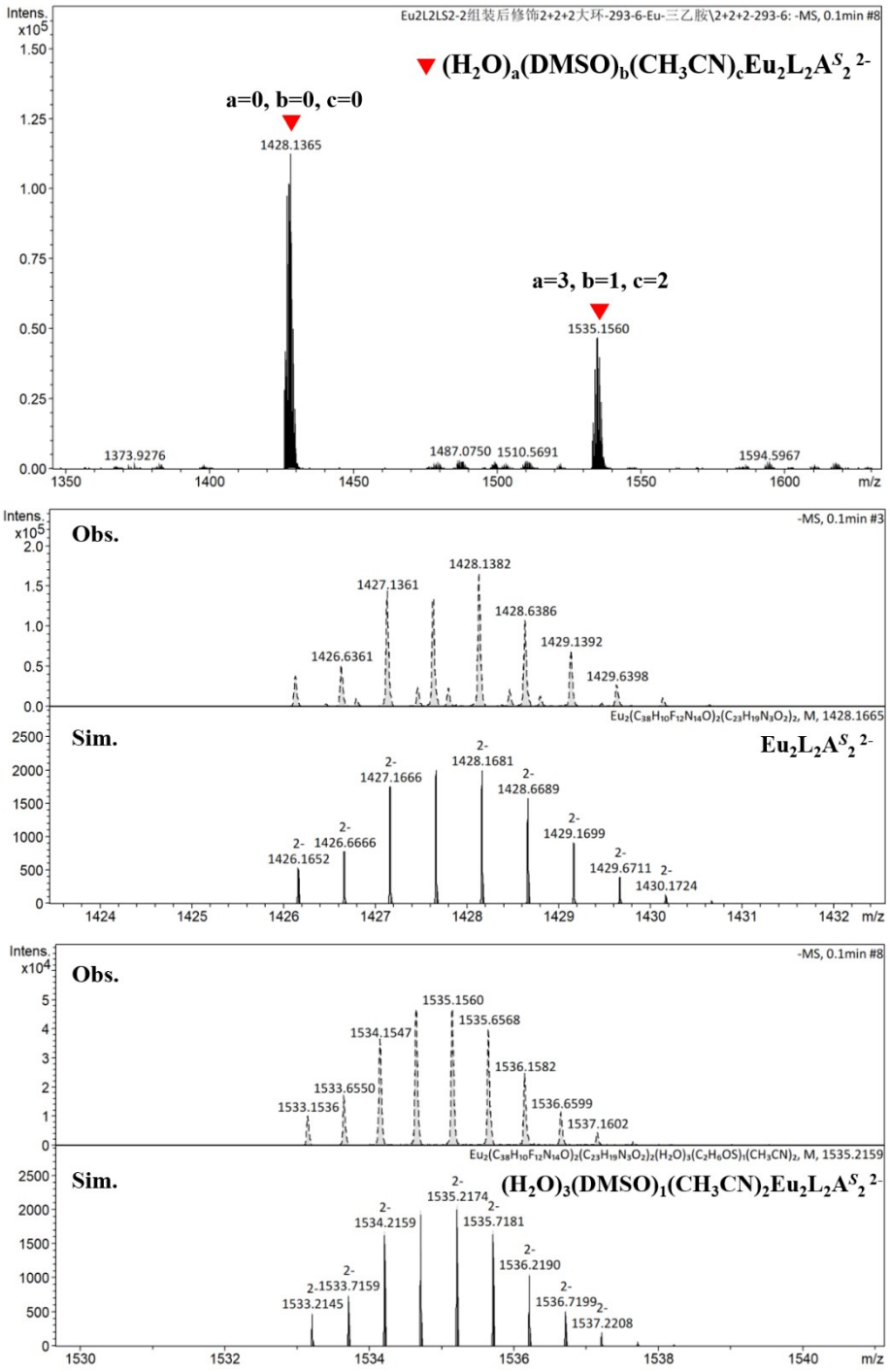

Figure S77. ESI-TOF-MS spectrum for $Eu_2L_2A^S_2$ in CH_3CN with insets showing the observed and calculated isotopic patterns of the peaks.

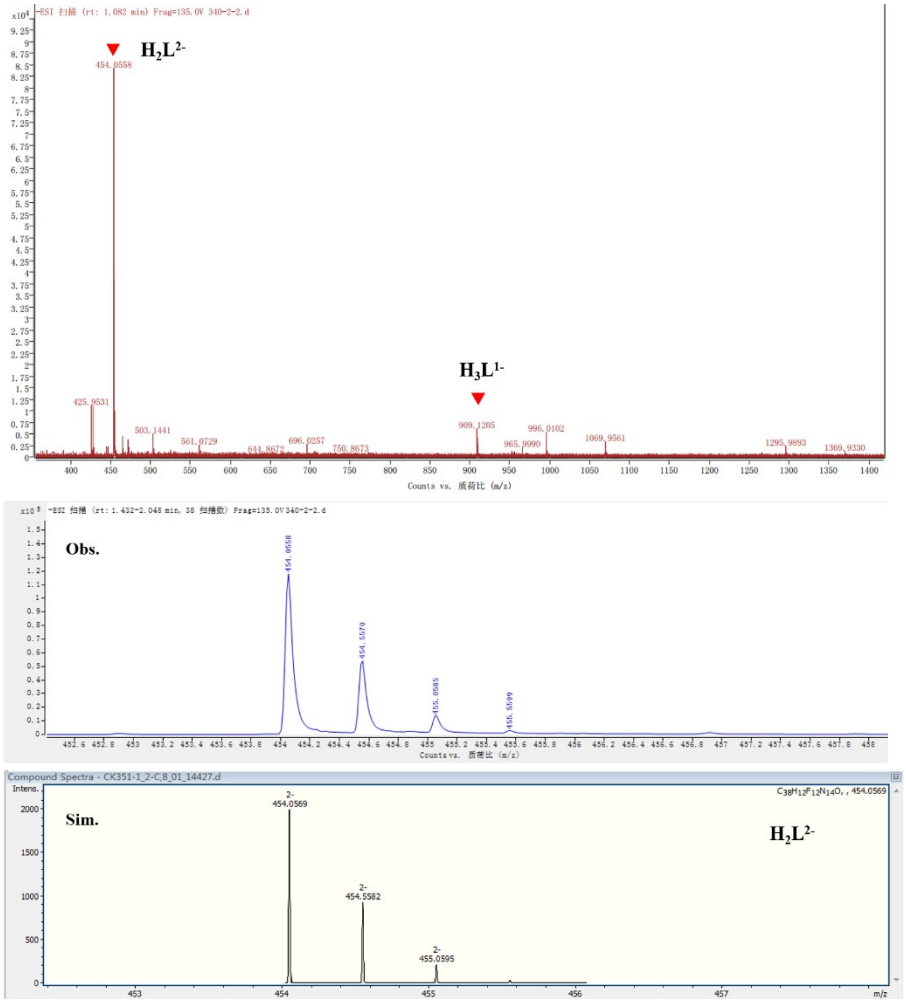

Figure S78. LC-QTOF-MS spectrum for Eu_2L_2 with 10 equiv OMA in H_2O(MS-neg) with insets showing the observed and calculated isotopic patterns of the peak.

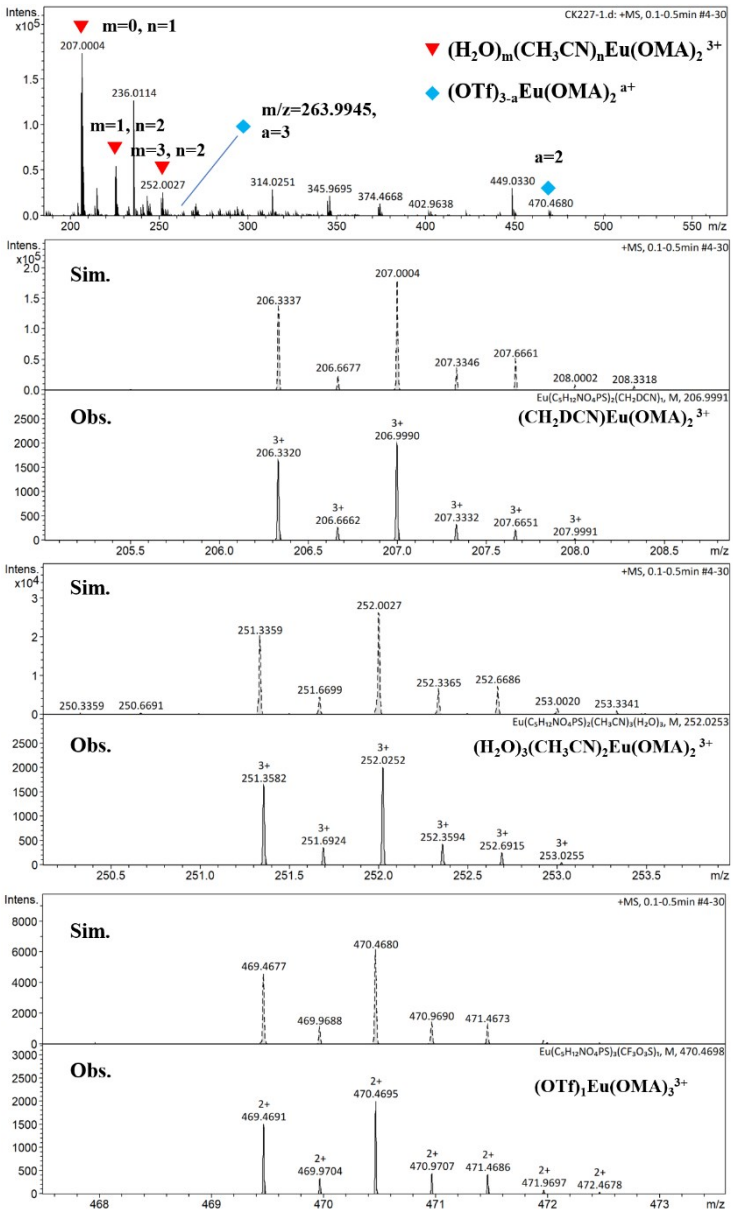

Figure S79. ESI-TOF-MS spectrum for Eu_2L_2 with 10 equiv OMA in H_2O (MS-pos) with insets showing the observed and calculated isotopic patterns of the peaks.

7 Single crystal X-ray diffraction studies

Single crystal of Europium mononuclear complex EuL'_2 was obtained by slow diffusion of chloroform into the acetonitrile solution of the complexes over several weeks. The X-ray diffraction studies for macrocycles were carried out on Bruker D8 VENTURE photon II diffractometer with Iμs 3.0 microfocus X-ray source using APEX III program.[5] Data reduction was performed with the SAINT and SADABS package. Both structures were solved by direct methods and refined by full-matrix least-squares on F2 with anisotropic displacement using the SHELX software package.[6] Solvent molecules were highly disordered and could not be reasonably located. These residual intensities were removed by PLATON/SQUEEZE routine.[7]

CCDC- 2065023 contains the supplementary crystallographic data for this paper. These data can be obtained free of charge via www.ccdc.cam.ac.uk/conts/retrieving.html (or from the Cambridge Crystallographic Data Centre, 12 Union Road, Cambridge CB21EZ, UK; fax: (+44) 1223-336-033; or deposit@ccdc.cam.ac.uk).

Table S2. Crystal data and structure refinement for EuL'$_2$.

Identification code	EuL'2	
Empirical formula	C22 H10 Br2 Eu F12 N14 O3[+ solvent]	
Formula weight	1058.21	
Temperature	150(2) K	
Wavelength	0.71073 Å	
Crystal system	Tetragonal	
Space group	$P4_32_12$	
Unit cell dimensions	a = 17.598(2) Å	α= 90°.
	b = 17.598(2) Å	β= 90°.
	c = 15.093(2) Å	γ = 90°.
Volume	4673.9(13) Å^3	
Z	4	
Density (calculated)	1.504 Mg/m^3	
Absorption coefficient	3.136 mm^{-1}	
F(000)	2020	
Crystal size	0.10 x 0.10 x 0.05 mm^3	
Theta range for data collection	2.315 to 21.724°.	
Index ranges	-18<=h<=18, -17<=k<=18, -15<=l<=15	
Reflections collected	16297	
Independent reflections	2763 [R(int) = 0.0911]	
Completeness to theta = 21.724°	99.7 %	
Absorption correction	Semi-empirical from equivalents	
Max. and min. transmission	0.7447 and 0.4808	
Refinement method	Full-matrix least-squares on F^2	
Data / restraints / parameters	2763 / 249 / 234	
Goodness-of-fit on F^2	1.094	
Final R indices [I>2sigma(I)]	R1 = 0.0853, wR2 = 0.2123	
R indices (all data)	R1 = 0.1002, wR2 = 0.2236	
Absolute structure parameter	0.039(13)	
Extinction coefficient	0.0058(11)	
Largest diff. peak and hole	2.992 and -2.062 e.Å^{-3}	

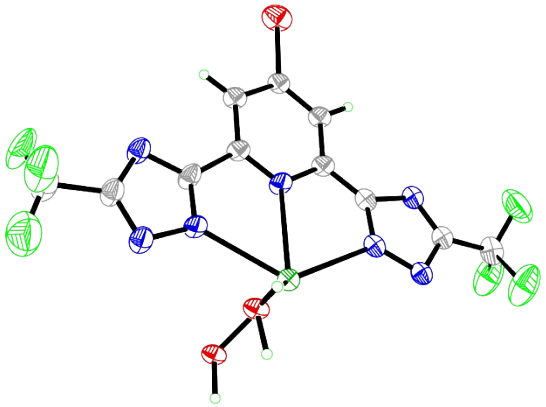

Figure S80. Ortep drawing of the asymmetric unit in the crystal structure of EuL'_2 at 30% probability level.

8 References

[1] Z. Wang, L.-P. Zhou, L.-X. Cai, C.-B. Tian and Q.-F. Sun, *Nano Research*, **2020**, 14, 398-403.

[2] Z. Tian, X. Yang, B. Liu, D. Zhong and G. Zhou, *Journal of Organometallic Chemistry*, **2019**, 895, 28-36.

[3] J. Sanning, P. R. Ewen, L. Stegemann, J. Schmidt, C. G. Daniliuc, T. Koch, N. L. Doltsinis, D. Wegner and C. A. Strassert, *Angew Chem Int Ed Engl*, **2015**, 54, 786-791.

[4] Horrocks, W. D. Jr.; Sudnick, D. R., *Acc. Chem. Res.* **1981**, 14, 384-392.

[5] APEX III, Data collection software (version 2017.3)

[6] G. M. Sheldrick, *Acta Crystallogr. Sect. A*, **2008**, 64, 112.

[7] A. L. Spek, *J. Appl. Crystallogr.* **2003**, 36, 7–13.